Some aspects of acousto-optical spectrum analysis

By:

Phys. Karla Janeth Sánchez Pérez

INAOE

A dissertation Submitted to the program in Optics.

Optics department.

In partial fulfillment of the requirements for the degree of

MASTER IN SCIENCES WITH SPECIALITY OF OPTICS

At

National Institute for Astrophysics Optics and Electronics

August 2011

Tonantzintla, Puebla.

Advisor:

PhD. Alexander S. Shcherbakov

INAOE researcher

Optics Departament

Thank God

Acknowledgements

I thank CONACyT for help me economically, with an scholarship and the financially support to this work (project # 61237).

I thank my advisor Dr. Alexander Shcherbakov for inviting me to work together, for his patience to explain and to answer questions, for his help in the development of this thesis with his academic and personal advices, for his dedication to this work to improve it as much as possible.

Thanks to my co-authors, Dr. Abraham Luna Castellanos, Dr. Alexej M. Bliznetsov, M.C. Daniel Sánchez Lucero, Dr. Jewgemij Maximov and Dr. Sergey A. Nemov.

Thanks to my PhD examiners, Dr. Abraham Luna Castellanos, Dr. Carlos G. Treviño Palacios and Dr. Julio C. Ramirez San Juan, for their help, support and advice.

I thank my mother Sonia Pérez P., my brother J. Carlos and all my family for their love and support.

Thanks to my husband Julio C. García for his help, patience and support in the hard times.

Anel Garza, Christian L. Alarcón, Jesús Emmanuel, Juan M. Carranza and Liliana Rivera, thanks for supporting me in the hard times and advising me in many others.

To my family

Resumen

La acusto-óptica es la rama de la Física que estudia los efectos de la interacción entre ondas acústicas y ópticas. Existen sistemas destinados al análisis de señales, tales sistemas necesitan dispositivos que permitan la interacción de ondas de sonido y de luz. La llegada del láser a principios de la década de los años 60 hizo posible, entre otras cosas, el uso del efecto acousto-óptico para modular la luz en casos de transmisión de señales. Sin embargo, para el correcto funcionamiento de dichos sistemas es necesario caracterizar los materiales en los cuales se llevará a cabo la interacción acusto-óptica.

Es necesario analizar los materiales, con los que se desea fabricar dispositivos acusto ópticos, para determinar si serń útiles en el análisis de señales. En este trabajo se presenta el estudio realizado sobre dos celdas acusto-ópticas destinadas al análisis de señales ópticas y señales de radio, dichas celdas acusto-ópticas están fabricadas de molibdato de calcio y KRS-5, respectivamente.

Abstract

Acousto-optics is the branch of physics devoted to the study of the effects of the interaction between acoustic and optical waves. For signal analysis systems, that allow the interaction of sound and light waves, acousto-optical devices are needed. The advent of lasers made possible, among other things, the practical use of acousto-optical effect to modulate light for signal transmission and manipulation. It is necessary to characterize the materials, in which the acousto-optical interaction will be hold, for the proper functioning of these systems.

To determine the usefulness of acousto-optical devices it is necessary to understand the properties of acousto-optical materials, wich are desirable to make acousto-optical devices. This thesis presents the study of two acousto-optical cells for optical signal and radio signal analysis, namely calcium molybdate and KRS-5 single crystals, respectively.

Contents

Chapter 1

Introduction

Acousto-optics is a branch of physics which studies the interaction between both acoustic and optic waves. Both optics and acustic have a history of almost same duration. Nevertheless, the acousto-optic effect has had a relatively short history, beginning with Brillouin predicting the diffraction of light by an acoustic wave being propagated in a medium of interaction, in 1922 [1]. In the past decades great progress has been made in acousto-optics, and now it is a widely used technique in the field of signal processing [2,3]. Acousto-optics has progressed thanks to several technological developments in different areas. The first important developmet was the laser [4], which has made available sources of intense monochromatic coherent light. The laser made the acousto-optic effect easier to observe and measure. A second area of developments has been dedicated to the search of new materials to fabricate acoustic wave devices. The research of transducer design has allowed the development of large-bandwidth, large aperture delay lines with good light-diffraction efficiency. Moreover, a notable portion of modern technical achievements in a high-bit-rate optical data processing is directly connected with utilizing such nonlinear phenomena as, for example, wave-mixing, various cross-and self-actions, etc. [5, 6]. Recently, two-cascade processing based on a three-wave interaction between coherent waves of different natures (optical and non-optical) had been successfully realized [7]. Then, in parallel, potential performances connected with using a collinear wave mixing in the specific case of

a medium without any group-velocity dispersion with strongly dispersive losses had been demonstrated [8, 9]. Both optical and radio wave signals will be analyzed. The techniques used for this purpose involve the use of acousto optical filters (AOFs) and heterodyning process.

In 1970-80s, novel optical spectral devices, known as electronically tunable acousto-optical filters had been proposed and developed. During these years AOFs have been remarkably progressed and widely exploited, for instance, in astrophysical observations. The principle behind the operation of acousto-optic filters is based on the diffracted light wavelength being dependent on the acoustic frequency. By tuning the frequency of the acoustic wave, the desired wavelength of the optical wave can be acousto-optically diffracted. There are two types of acousto-optic filters, the collinear and non-collinear filters. The type of filter depends on geometry of acousto-optic interaction. Collinear acousto-optical interaction was initially predicted and studied in the middle of sixties by R.W. Dixon [10]. An advanced collinear acousto-optical filter, based on a calcium molybdate ($CaMoO_4$) single-crystal, is used to analyze the optical signals.

Heterodyning is a radio signal processing technique invented in 1901 by Reginald Fessenden. In heterodyning process high frequency signals are converted to lower frequencies by combining two frequencies. [11]

Heterodyning is useful for frequency shifting information of interest into a useful frequency range following modulation or prior to demodulation. In our case, the two frequencies are combined in the AO cell. Heterodyning creates two new frequencies, according to the properties of the sine function; one is the sum of the two frequencies mixed, the other is their difference. These new frequencies are called heterodynes. Typically only one of the new frequencies is desired, the higher one after modulation or the lower one after demodulation. The other signal is filtered out of the output of the mixer. Heterodyning is widely used in communications engineering to generate new frequencies and move information from one frequency channel to another. The technique proposed, to analyze the

radio wave signals, implies a two-stage integrated processing, these are the wave heterodyning and the optical processing in the same solid state cell. A thallium bromine-thallium iodine (TlBr-TlI) solution, which forms KRS-5 cubic-symmetry crystals with the mass-ratio 58% of TlBr to 42% of TlI, is used to analyze this radio wave signals.

In both acousto-optical filter and heterodyning techniques, for spectrum analysis process, there are several kind of devices involved. These are lasers, lens arrays, acousto-optical cells, detectors, etc. The acousto-optical cell allows the interaction between the optical wave, coming from the laser, and the ultrasonic wave generated by the piezotransducer attached to the material. The acustic wave changes the refraction index troughout the crystalline material within the cell, see figure 1.1. The changes in the index refraction cause that the material act as a diffraction grating.

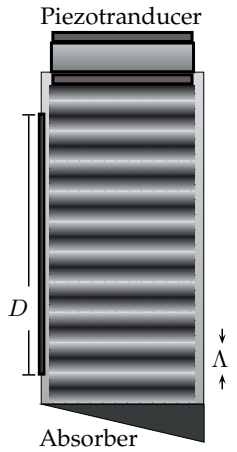

Figure 1.1: An acousto-optic cell. A piezoelectric transducer creates sound waves in the material, the refraction index changes and the material acts as a diffraction grating. The light beam is diffracted into +1 order.

In the Bragg regime, after the expanded beam light fit through the aperture of the cell, is possible to observe only two diffraction orders going out of the opposite face of the cell. Those diffraction orders are collected by a positive lens, which focuses them on the surface of a detector.

In this work, some aspects of the acousto-optical spectrum analysis are considered . The bandwidth, frequency resolution and efficiency of acousto-optical interaction, for both $CaMoO_4$ and KRS-5 single crystals, are estimated. Also, within the KRS-5 cell, a two cascade algorithm of processing will be exploited for direct parallel and precise optical spectrum analysis. It is necessary estimate the technical requirements to performance data of the acousto-optical cell as well as to acceptable values of the operating frequencies.

Chapter 2

Acousto-optic effect and some considerations

2.1 Introduction

Acousto-optic devices use the interaction between light and an ultrasonic waves [12]. When a sound wave is applied inside of a material, with initial refractive index n, the atoms are displaced, forming layers of different density. In other words, in acousto-optic materials the ultrasonic wave induces refractive index changes caused by the photoelastic effect. Those changes have the periodicity, amplitude and phase modulation of the acoustic wave, and they act as a phase grating to diffract the incident optical beam.

The elastic and acoustic behaviour of the materials will be taken into acount in this section, because of that is necesary to solve the problem mentioned in the last chapter.

2.2 Elastic properties of crystals

All kind of materials in the nature are comformed by atoms, which are highly mobile within their structure. Inside of a crystalline acousto-optical material the atoms are slightly displaced, from its structure, when it is applied an external

force. The concepts like stress, strain, elasticity, etc. help to understand what happens to the material when it is under the action of an external force. The elasticity of crystals also determines their optical behaviour, such a behaviour with penetrating light is characteristic for each crystal.

2.2.1 The stress tensor

When a body is under the action of external forces, it is said that the body is in a state of stress. Considering a volume element located within the stressed body, one may recognize two types of forces acting on it. There are body-forces which act throughout the body on all its elements and whose magnitudes are proportional to the volume of the element. There are forces exerted on the surface of the element of volume caused by the material surrounding it, and they are proportional to the area of the surface of the element. The force per unit area is called the stress [13] and it is denoted by σ. A stress is said to be homogeneous if the forces acting on the surface of an element of fixed shape and orientation are independent of the position of the element in the body.

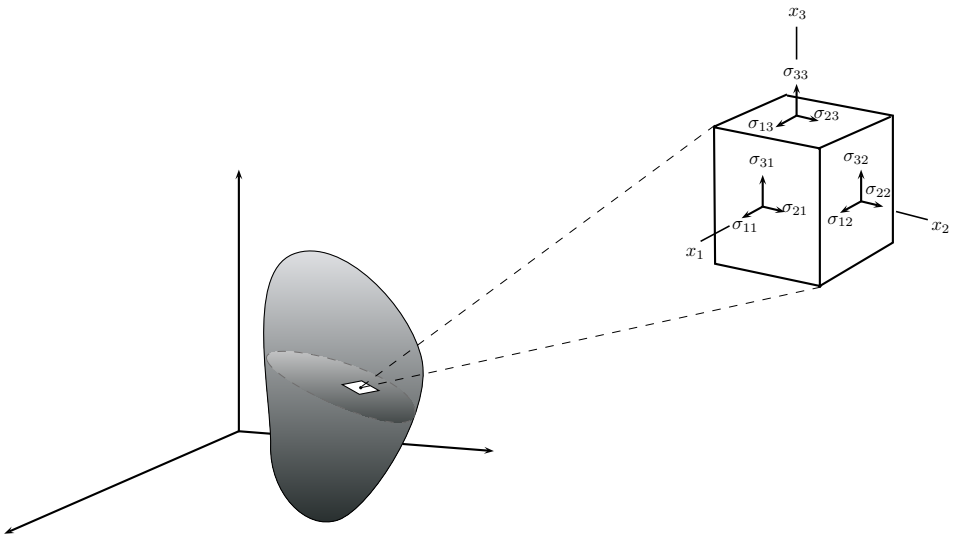

Figure 2.1: The forces on the faces of a unit cube in a stressed body.

Now, focusing to states in which: 1) The stress is homogeneuos troughout the body, 2) All parts of the body are in statical equillibrium and 3) There are no body-forces or body-torques, it will be possible to analize the stress effect on a body. Figure 2.1 shows a unite cube within a body. Its edges are parallel to the axes Ox_1, Ox_2, Ox_3. The material outside the unite cube exerts a force, that is transmitted across each face of the cube, upon the material inside the cube. The force transmitted across each face may be resolved into three components. First, consider the three faces which are towards the three positive ends of the axes. σ_{ij} denotes the component of force in the $+Ox_i$ direction transmitted across that face of the cube which is perpendicular to Ox_j.

Because of the stress is homogeneous the forces exerted on the cube across the three opposite faces must be equal and opposite to those shown in the figure 2.1. σ_{11}, σ_{22}, σ_{33} are the normal components of stress and σ_{12}, σ_{21}, σ_{23}, etc. are the shear components. σ_{ij} form a second-rank tensor.

The assumtion (2) imposes conditions on the σ_{ij}. Taking moments about an axis parallel to Ox_1 passing troughout the centre of the unit cube, see Fig. 2.2.

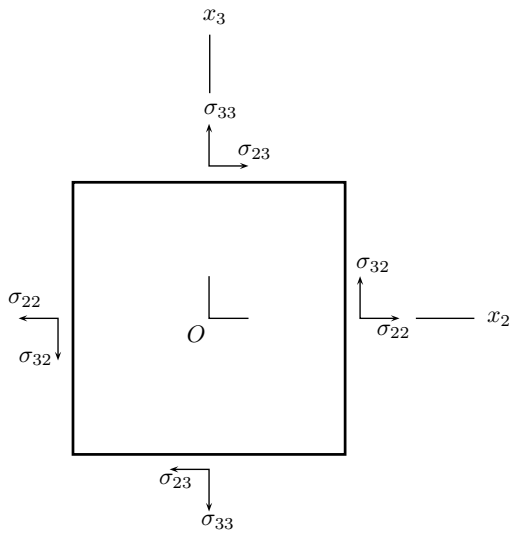

Figure 2.2: Forces on the face of a unit cube in a stressed body. The axis Ox_1 is perpendicular to the page.

Because the stress is homogeneous, the three components of force on any face

all pass through the mid-point of the face, then all the components on the Ox_1 faces give no moment. Therefore it is found the condition for equilibrium

$$\sigma_{ij} = \sigma_{ji} \tag{2.2.1}$$

This relation holds even if the stress is inhomogeneous, the body is not in statical equilibrium, and body forces are present, provided body-torques are not present.

2.2.2 The strain tensor

One can consider an acoustic wave propagating through a crystaline material. The atoms, which conform the crystalline structure, vibrate parallel to the direction of the wave propagation. Now, $\vec{k} = k\vec{m}$ is the acoustic-wave propagation vector and $\vec{U} = U\vec{u}$ is the vector that represents the motion of the atoms. The strain tensor γ can be obtained by calculating a dyadic product

$$\gamma = \frac{1}{2} kU \left\{ \vec{m} \cdot \vec{u} + \vec{u} \cdot \vec{m} \right\} \tag{2.2.2}$$

To write 2.2.2 in the matrix notation, one can substitute as follows

$$\gamma = \begin{pmatrix} \gamma_{11} & 2\gamma_{12} & 2\gamma_{13} \\ 2\gamma_{21} & \gamma_{22} & 2\gamma_{23} \\ 2\gamma_{31} & 2\gamma_{32} & \gamma_{33} \end{pmatrix} \rightarrow \gamma = \begin{pmatrix} \gamma_1 & \gamma_6 & \gamma_5 \\ \gamma_6 & \gamma_2 & \gamma_4 \\ \gamma_5 & \gamma_4 & \gamma_3 \end{pmatrix} \rightarrow \bar{\gamma} = (\gamma_1 \, , \gamma_2 \, , \gamma_3 \, , \gamma_4 \, , \gamma_5 \, , \gamma_6)$$

Now, it is considered that the wave normal ort (unit vector) $\vec{m}$ is passing along the [100]-axis, while the vector $\vec{u}$, of the transversal elastic displacements, is oriented along the [001]-axis in the crystalline material, i.e. $\vec{m} = [1\,0\,0]$ and $\vec{u} = [0\,0\,1]$. Then it is obtained the deformation tensor γ

$$\gamma = \frac{\gamma_0}{2} \begin{pmatrix} 0 & 0 & 1 \\ 0 & 0 & 0 \\ 1 & 0 & 0 \end{pmatrix} \tag{2.2.3}$$

In this case the atoms of the crystal are vibrating perpendicularly to the acoustic wave propagation, this is an example of shear strain. γ_0 is the amplitude of the

shear deformation. Now, the tensor γ of the second rank with the components γ_{kl} with k, l =1,2,3 can be converted[1] into a 6-dimension vector $\bar{\gamma} = \gamma\,(0, 0, 0, 0, 1, 0)$ with the components $\bar{\gamma}_\mu$ where $\mu = 1, 2, ..., 6$, using the matrix notation [13, 14], which includes re-notating $\bar{\gamma}_\mu = \gamma_{kk}$ with $\mu = 1, 2, 3$ and $\bar{\gamma}_\mu = 2\gamma_{kl}$ where $k \neq l$, $\mu = 4, 5, 6$.

Taking the wave vector $\vec{K}$ and the displacement vector $\vec{u} = u\vec{m}$, when these waves are passing along the crystallographic axis [111], so that $\vec{K} \parallel \vec{m} \parallel [1\,1\,1]$. Due to $\vec{K} \parallel$[111] and $\vec{u} \parallel$[111], one can write $\vec{q} = \vec{K}/|\vec{K}| = (1/\sqrt{3})$(1,1,1) and $\vec{u} = (1/\sqrt{3})$(1,1,1), so that the corresponding deformation tensor γ takes the form

$$\gamma = \frac{1}{3}\begin{pmatrix} 1 & 1 & 1 \\ 1 & 1 & 1 \\ 1 & 1 & 1 \end{pmatrix} \tag{2.2.4}$$

The tensor γ converted into a 6-dimension vector is $\bar{\gamma} = (1/\sqrt{3})\ (1, 1, 1, 2, 2, 2)$. This example shows the linear combination of both longitudinal and shear strain.

2.2.3 Elasticity

The elastic property of a crystal is a relation between stress and strain, which are examples of a second-rank tensor and thus sensitive to direction [15]. When a solid body is under the act of stress forces, the body changes its shape; but if the applied stress is below of the elastic limit, then the strain is recoverable, namely, the body returns to its shape. It has been observed, that for sufficiently small stresses, the amount of strain is proportional to the magnitude of the applied stress [13].

[1]This change is realized to make possible to calculate the product between the stress and photoelastic tensors. See sections 3.4 and 4.2

Hooke's Law

The Hook's law states that in an elastic solid the strain is directly proportional to the stress. Nevertheless this law applies to small strains only [13, 16].

It is seen that a both homogeneous stress and strain are each specified, in general, by second-rank tensors, now the generalized form of Hook's Law is written by

$$\gamma_{ij} = s_{ijkl}\sigma_{kl} \tag{2.2.5}$$

where s_{ijkl} are the compliances of the crystal and σ_{ij} are the stresses. The elastic stiffness constants and the elastic compliance constants are fourth-rank tensors.

As an alternative to below-mentioned equations, the stresses can be expressed in terms of the strains by the equations

$$\sigma_{ij} = c_{ijkl}\gamma_{kl} \tag{2.2.6}$$

here the c_{ijlk} are the stiffness constants of the crystal.

Due to the symmetry [13] in the suffixes of s_{ijkl} and c_{ijkl} ($ijkl = jilk, ijkl = jikl$), it is possible to use the matrix notation for stress and strain tensors, then them take the shorter form

$$\gamma_i = s_{ij}\sigma_j, \qquad (i, j = 1, 2, ..., 6) \tag{2.2.7}$$

and,

$$\sigma_i = c_{ij}\gamma_j, \qquad (i, j = 1, 2, ..., 6) \tag{2.2.8}$$

The effective elastic modulus C can be obtained by

$$C = \gamma_i c_{ij} \gamma_j \tag{2.2.9}$$

2.2.4 Piezoelectricity

When a stress is applied to certain crystals, they develop an electric moment. Its magnitude is proportional to the applied stress and it is called the direct

piezoelectric effect. The polarization charge per unit area is given by [13]

$$P_i = d_{ijk}\sigma_{jk} \tag{2.2.10}$$

where d is the piezoelectric tensor.

When an electric field is applied in a piezoelectric crystal the shape of the crystal changes slightly, this phenomenon is called the converse piezoelectric effect. The components of the electric field E_i within the crystal are linearly related with the components of the strain tensor γ_{ij} by

$$\gamma_{jk} = d_{ijk}E_i \tag{2.2.11}$$

Writing the above-mentioned equation in its matrix form, it is obtained

$$\gamma_j = d_{ij}E_i \qquad (i = 1, 2, 3; j = 1, 2, ..., 6) \tag{2.2.12}$$

The discovery of the direct piezoelectric effect is credited to the Curie brothers. Nevertheless, the converse piezoelectric effect was mathematically deduced, from the fundamental thermodynamic principles, by Lippmann (1881). The existence of the converse effect was immediately confirmed by Curie brothers in the following publication (1881) [17–19].

Piezotransducer

Piezotransducer is a device that converts one type of energy to another by taking advantage of the piezoelectric properties of materials, such a device can be used for several purposes, but in generally the piezotransducers can be used to both convert electricity into ultrasonic waves as well as convert ultrasonic waves into electricity. When electricity is applied to a piezotransducer in the form of an alternating current, positive and negatives charges within the element repeatedly repel and attract each other in a way that causes the piezotransducer to vibrate. As the piezotransducer vibrates, the air around it is displaced and a high pitch sound is created in the form of ultrasonic sound waves [17].

2.3 Acousto-optical interaction

The interaction within an acousto-optical cell involves the wave vectors $\vec{k_0}$ and $\vec{k_1}$ related by $\vec{k_1} = \vec{k_0} + \vec{K}$. The are two types of acousto-optical interaction, these are non-collinear and collinear interaction. Each one depends of the direction of these vectors. The parameters peculiar to the material affect the efficiency, bandwidth and aperture size. Most good acousto-optic materials have been identified by noting the strong dependence of figures of merit M_2 (see section 2.3.1), on the index of refraction n and acoustic velocity V [20]. To find the maximal values of M_2 for a given material requires detailed calculations, as one can see on chapters 3 and 4

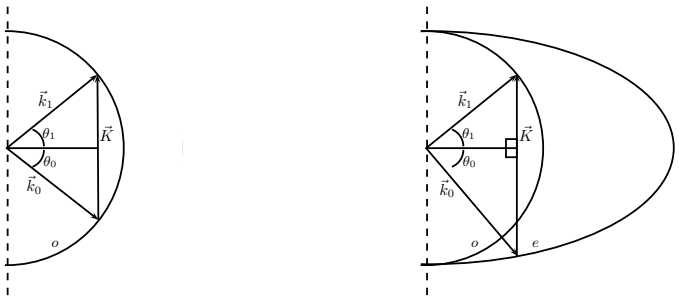

(a) (b)

Figure 2.3: Acousto-optical interaction. (a) Isotropic diffraction. (b) Anisotropic diffraction

2.3.1 Photoelasticity

The refractive index, permittivity and dielectric constants are in general functions not only of the applied electric field, but also of the stress on the crystal. The change of refractive index caused by stress is called the photoelastic effect [13].

The stress-optical coefficients deal with the photo-elastic behaviour and give the relation between the optical coefficients of the crystal and the components of an applied stress tensor. Their maximum number is 36 and this number remains

undiminished in the triclinic system of crystals because the relation $c_{ij} = c_{ji}$ does not generally hold good for stress-optical coefficients. Just as in the case of optical coefficients, the largest number of moduli of elasticity and of stress-optical coefficients that are required in each case depends on the symmetry properties of the crystal in question [21].

Here is shown the photo-elastic tensor p, of the fourth rank, taken and converted into the form of a 6×6 matrix with the components $p_{\lambda\mu}$. In the particular case of a $CaMoO_4$-crystal, whose point symmetry group is 4/m, one can write [14]

$$p_{\lambda\mu} = \begin{pmatrix} p_{11} & p_{12} & p_{13} & 0 & 0 & p_{16} \\ p_{12} & p_{11} & p_{13} & 0 & 0 & -p_{16} \\ p_{31} & p_{31} & p_{33} & 0 & 0 & 0 \\ 0 & 0 & 0 & p_{44} & p_{45} & 0 \\ 0 & 0 & 0 & -p_{45} & p_{44} & 0 \\ p_{61} & -p_{61} & 0 & 0 & 0 & p_{66} \end{pmatrix} \tag{2.3.1}$$

Where $p_{11} = 0.17$,$p_{12} = -0.15$, $p_{13} = -0.08$, $p_{16} = 0.03$, $p_{31} = 0.10$, $p_{33} = 0.08$, $p_{44} = 0.06$, $p_{45} = 0.06$, $p_{61} = 0.10$, $p_{66} = 0.03$.

For the cubic KRS-5 crystal, whose point symmetry group is m3m, the matrix representation for the tensor p is

$$p_{\lambda\mu} = \begin{pmatrix} p_{11} & p_{12} & p_{12} & 0 & 0 & 0 \\ p_{12} & p_{11} & p_{12} & 0 & 0 & 0 \\ p_{12} & p_{12} & p_{11} & 0 & 0 & 0 \\ 0 & 0 & 0 & p_{44} & 0 & 0 \\ 0 & 0 & 0 & 0 & p_{44} & 0 \\ 0 & 0 & 0 & 0 & 0 & p_{44} \end{pmatrix} \tag{2.3.2}$$

Where $p_{11} = 0.21$, $p_{12} = 0.22$, and $p_{44} = 0.15$.

Acousto-optical figures of merit

A large acousto-optical figure of merit is desired for device applications. The interes in practical applications of acousto-optics caused a demand for more sensitive acousto-optic materials, and thus, the study of acousto-optic materials emphasizes on the device optimization. There are several AO figures of merit that have been used for judging the usefulness of an AO material. The relevant one to be used depends on the specific applications. Smith and Korpel proposed a figure of merit for difraction merit for difraction efficiency [22] and other figures of merit addressing different aspects, such a bandwidth optimization and resolution were also proposed [23, 24]. Several AO figures of merit are defined in the literature. These include [3, 12, 22, 25]

$$M_1 = \frac{n^7\, p^2}{\rho\, V} \qquad M_2 = \frac{n^6\, p^2}{\rho\, V^3} \qquad M_3 = \frac{n^7\, p^2}{\rho\, V^2} \qquad M_4 = \frac{n^8\, p^2\, V}{\rho} \qquad M_5 = \frac{n^8\, p^2}{\rho\, V^3}$$

n is the refraction index, p is the photoelastic constant, ρ is the material density, and V is the acoustic wave velocity. These figures of merit are generally listed as the normalized quantities M (normalized to values for fused silica).

The acoustic figure of merit is one of the fundamental parameters in materials selection. M_2 is the AO figure of merit most often referred to in the literature and is widely used for the comparison of AO materials. This is a misconception, since from the viewpoint of device applications, M_2 is usually not appropriate. Comparison of AO materials (or modes) based on M_2 can lead to erroneous conclusions.

M_1. This quantity can be considered as the figure of merit of the material when the efficiency-bandwidth product is an important criterion [25, 26]. The modulator bandwidth is an important design parameter, this is why the factor M_1 provides a useful figure of merit for materials to be used in modulators and deflectors [27].

M_2. The constant M_2 is related to material properties, it is useful for estimating the efficiency of the acousto-optic diffraction. It shows the relation between

the diffracted light power and the acoustic wave intensity. M_2 is used only when efficiency is the only parameter of concern.

M_3**.** This constant is relevant for optimized efficiency for a specified bandwidth and aperture time, because of in the design of AO deflectors, or Bragg cells, besides efficiency and bandwidth, a third parameter of interest is the aperture time t. A minimum acoustic beam height H must be chosen to ensure that the aperture is within the near field of the acoustic radiation.

M_4**.** This is the appropriate acousto-optical figure of merit when the acoustic power density is the limiting factor.

M_5**.** In the design of acousto-optical tunable filters, the parameters to be optimized are the product of efficiency η, the resolving power $\lambda_0/\Delta\lambda$, and the solid angular aperture $\Delta\Omega$. In this case the appropriate AO figure of merit is M_5.

2.3.2 Bragg diffraction

In a grating there are generally two regimes, known as Raman-Nath and Bragg, based on the number of diffraction orders. In Bragg regime only one diffraction order persists, in this case some 95% of incident light power is concentrated in the first diffraction order [28]. In Raman-Nath regime there are multiple diffraction orders, but the existence of multiple orders is usually not technologically desirable [29]. The distinction between Raman-Nath and Bragg diffraction regimes is given by the diffraction parameter Q, introduced by Klein and Cook [30]

$$Q = \frac{2\pi\lambda l}{n\Lambda^2} \tag{2.3.3}$$

l is the acousto-optical interaction length, n is the refraction index.

When $Q < 1$, the Raman-Nath regime takes place, and when $Q >> 1$ the diffraction is said to be in the Bragg regime, in this mode is required high sound frequency and adequate interaction length. The intermediate region where $1 < Q < 10$ gives a mixture of the characteristics of both Raman-Nath and Bragg regimes [3].

In an isotropic medium, the maximun diffraction efficiency is obtained when the incident light direction is at an angle θ_B to the acoustic wavefront. The principle of momentum conservation requires that the acoustic and optical wave vectors form a closed triangle. For isotropic AO diffraction the triangle is isosceles (see Fig.2.3(a)), and the incident and diffracted optical wave vectors make the same angle with the acoustic wavefront at the Bragg angle, which is given by [3,25]

$$\sin\theta_B = \frac{\lambda}{2\,n\,\Lambda} = \frac{\lambda f}{2\,n\,V} \tag{2.3.4}$$

Where λ and Λ are the light and acoustic wavelengths, respectively, n is the refraction index, V is the acoustic velocity and f is the acoustic frequency.

Considering that the acousto-optical interaction occurs in an anisotropic uniaxial crystal, then there are an ordinary optical wave and an extraordinary optical wave. The refraction indices depend of the direction of propagation and the polarization of the optical wave. The acoustic wave could couple the incident and diffracted optical wave of the same polarization or orthogonal polarization.

Applying the law of cosine to the triangle (see fig.2.3(b)), then the following pair of equations, for the incident and diffraction angle, are obtained.

$$\sin\theta_{0,1} = \frac{\lambda\,f}{2\,n_{0,1}\,V}\left[1 + \frac{V^2}{\lambda^2\,f^2}\left(n_0^2 - n_1^2\right)\right] \tag{2.3.5}$$

$n_{0,1}$ are the refractive indices for the incident and diffracted light, respectively.

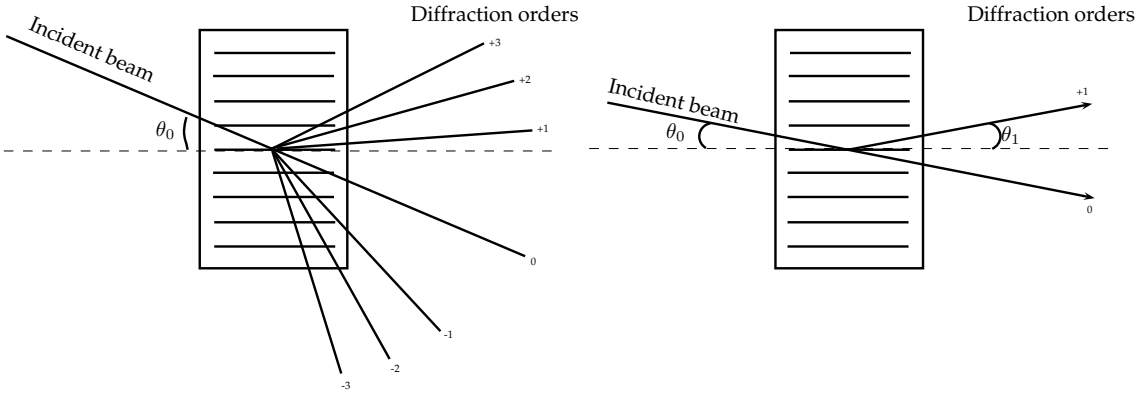

Figure 2.4: This figure shows both Raman-Nath and Bragg regimes

2.3.3 Non-collinear acousto-optical interaction

Non-collinear interaction, within an acousto-optical cell, involves the wave vectors $\vec{k}_0$, for incident optical wave, and $\vec{k}_1$, for scattered optical wave. These vectors are related by $\vec{k}_1 = \vec{k}_0 + \vec{K}$. There are two cases in the non-collinear process, these cases are normal and anomalous scattering. Normal scattering is obtained when $\vec{k}_0$, $\vec{k}_1$ and $\vec{K}$ have the same polarization state. Anomalous dispersion is given by a change in the polarization state of those vectors. The change in polarization state of $\vec{k}_0$, $\vec{k}_1$ and $\vec{K}$ is caused by a transition between ordinary (o) to extraordinary (e) surface or vice versa. Figures 2.5 and 2.6 show both normal and anomalous scattering cases in an uniaxial crystal.

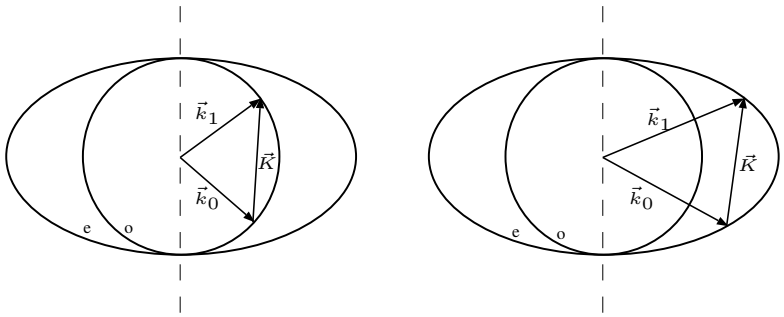

Figure 2.5: Normal dispersion in an uniaxial crystal for non-collinear case

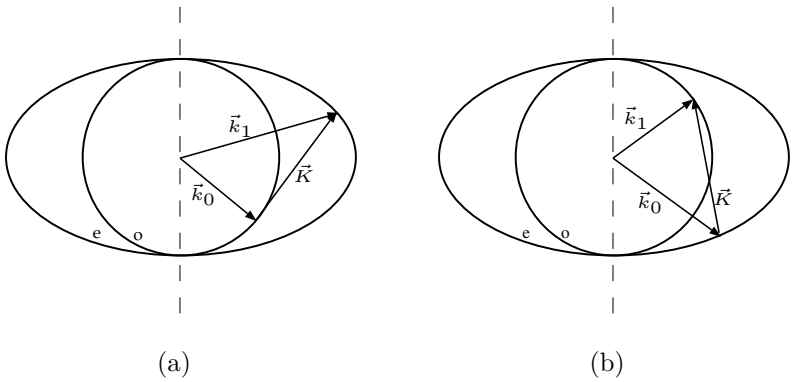

Figure 2.6: Anomalous dispersion in an uniaxial crystal for non-collinear case

2.3.4 Collinear acousto-optical interaction

One have collinear interaction when the wave vectors $\vec{k_0}$ and $\vec{k_1}$ are on the same line. The are two kind of collinear process, they are the forward and backward cases, see Figure 2.7. Forward process will be considered.

Forward process

When the frequency f of acoustic wave is less than a few gigahertz, so called regime of the forward scattering takes place, and the wave vectors $\vec{k_0}$ and $\vec{k_1}$ are oriented co-directionally. During such a process, the wave vectors $\vec{k_0}$ and $\vec{k_1}$ of the incident and scattered light beams lie along the acoustic wave vector $\vec{K}$, so that one can consider a scalar equality $k_1 = k_0 + K$ for modulus of the corresponding vectors. This scalar relation can be rewritten together with the needed equality for frequencies as

$$\frac{n(\lambda_1)}{\lambda_1} = \frac{n(\lambda_0)}{\lambda_0} + \frac{f}{V} \tag{2.3.6a}$$

$$\nu_1 = \nu_0 + f \tag{2.3.6b}$$

where $f << \nu_{0,1}$.

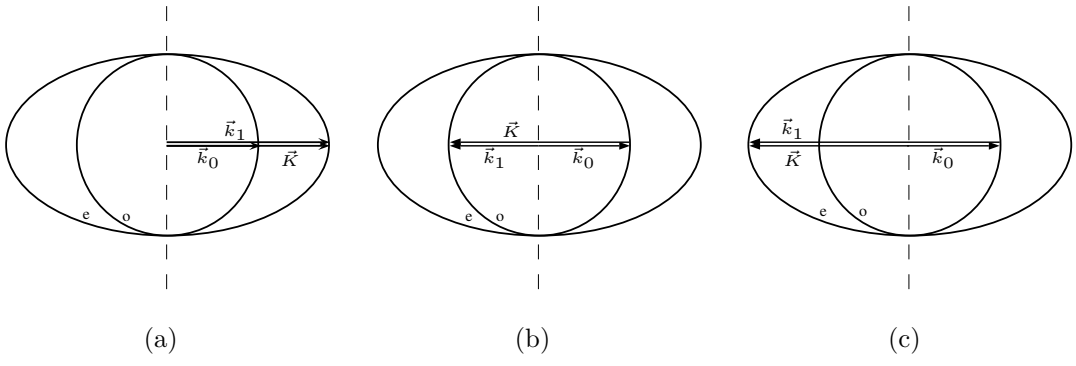

Figure 2.7: Normal and anomalous dispersion in an uniaxial crystal for collinear case. a) shows forward anomalous process, b) and c) belong to normal and anomalous backward process

2.4 Conclusions

The selection of acousto-optic materials depends on the specific device application, namely, some material could be used for one type of device, but maybe the same material is not applicable for another, for example, an optically isotropic material can not be used for tunable filter purposes. The obtained information, about the elastic and acoustic behaviour of the materials, makes possible to consider a few estimations related to device design and how to exploit it to take it on both optical and radio wave signal analysis. This knowledge will allow to determinate if both calcium molybdate and KRS-5 single crystals are useful for acousto-optical spectrum analysis. Such analysis is shown in chapters 3 and 4, respectively.

Chapter 3

Acousto-optical spectrum analysis of optical signals using a collinear filter

3.1 Introduction

In this chapter is devoloped the exact and closed analytical model of the collinear light scattering by continuous acoustic waves in birefringent crystals with the presence of both the acoustic attenuation and divergence the acoustic beam. The difference between the velocities of light and ultrasound gives an opportunity for applying the quasi-stationary approximation.

3.2 Potential contribution of the dispersion

Consider the collinear geometry of stationary Bragg light scattering by coherent acoustic wave in an optically dispersive medium, and take into account the Eqs. 2.3.6a and 2.3.6b. One can expand both $n(\lambda_1)$ and λ_1^{-1} from Eq.2.3.6a in

power series respect to λ in the vecinity of a point λ_0. This means that

$$n(\lambda_1) \approx n(\lambda_0) + \left(\frac{\partial n}{\partial \lambda}\right)_{\lambda_0} \Delta\lambda + \frac{1}{2}\left(\frac{\partial^2 n}{\partial \lambda^2}\right)_{\lambda_0} \Delta\lambda^2 \tag{3.2.1a}$$

$$\frac{1}{\lambda_1} = \frac{1}{\lambda_0 + \Delta\lambda} \approx \frac{1}{\lambda_0}\left(1 - \frac{\Delta\lambda}{\lambda_0} + \frac{\Delta\lambda^2}{\lambda_0^2}\right) \tag{3.2.1b}$$

in the second approximation. Now, the are two options, which will be analized.

The first option supposes that the magnitude of $\Delta\lambda$ is determined only by parameters of a medium, so that $\Delta\lambda$ is perfectly independent on the magnitude of the acoustic frequency f and it can be arbitrary valued.

The second option allows a dependence of $\Delta\lambda$ on f, so that, due to $\lambda = c/\nu$ and $\Delta\nu = \nu_1 - \nu_0 = f$ (see Eq.2.3.6b), one can obtain that $\Delta\lambda = -c^{-1}\lambda^2\Delta\nu = -c^{-1}\lambda^2 f \approx -c^{-1}\lambda_0^2 f$. Because of the carrier acoustic frecuency is limited by $f < 10^{10}$Hz, $\lambda_0 \leq 10^{-4}$ cm for the visible range and $c = 3 \times 10^{10}$cm/s, one can obtain a small parameter $|\Delta\lambda/\lambda_0| \approx \lambda_0 f/c \leq 3 \times 10^{-5}$. In the second approximation relative to the above-estimated parameter $(\Delta\lambda/\lambda_0)$, the Eqs.3.2.1 convert the Eq.2.3.6a to

$$\begin{aligned}\frac{n(\lambda_1)}{\lambda_1} &= \frac{n(\lambda_0)}{\lambda_0} + \left(\frac{\partial n}{\partial \lambda}\right)_{\lambda_0}\frac{\Delta\lambda}{\lambda_0} + \frac{1}{2}\left(\frac{\partial^2 n}{\partial \lambda^2}\right)_{\lambda_0}\frac{\Delta\lambda^2}{\lambda_0} - n(\lambda_0)\frac{\Delta\lambda}{\lambda^2} \\ &\quad - \left(\frac{\partial n}{\partial \lambda}\right)_{\lambda_0}\frac{\Delta\lambda^2}{\lambda_0^2} - \frac{1}{2}\left(\frac{\partial^2 n}{\partial \lambda^2}\right)_{\lambda_0}\frac{\Delta\lambda^3}{\lambda_0^2} + n(\lambda_0)\frac{\Delta\lambda^2}{\lambda_0^3} \\ &\quad + \left(\frac{\partial n}{\partial \lambda}\right)_{\lambda_0}\frac{\Delta\lambda^3}{\lambda_0^3} + \frac{1}{2}\left(\frac{\partial^2 n}{\partial \lambda^2}\right)_{\lambda_0}\frac{\Delta\lambda^4}{\lambda_0^3} = \frac{n(\lambda_0)}{\lambda_0} + \frac{f}{V}\end{aligned} \tag{3.2.2}$$

Now the terms in equation 3.2.2 must be estimated.

Estimating the first derivative

The light group velocity V_g can be expressed as $V_g = \frac{c}{n_g} = c\left[n - \lambda\left(\frac{\partial n}{\partial \lambda}\right)_{\lambda_0}\right]^{-1}$, so that $n_g - n > 0$ and $n_g - n = -\lambda_0\left(\frac{\partial n}{\partial \lambda}\right)_{\lambda_0}$. The corresponding diagram for bulk fused silica is depicted in figure 3.1. It is seen [31] from figure 3.1 that

$n_g - n \in [0.015, 0.030]$ when λ_0 is varied from about 1000nm to 500nm. This means that for $\lambda_0 \approx 500$ nm one can take the estimating value of about

$$|n_g - n| = \left| \lambda_0 \left(\frac{\partial n}{\partial \lambda} \right)_{\lambda_0} \right| \leq 3 \times 10^{-2} \tag{3.2.3}$$

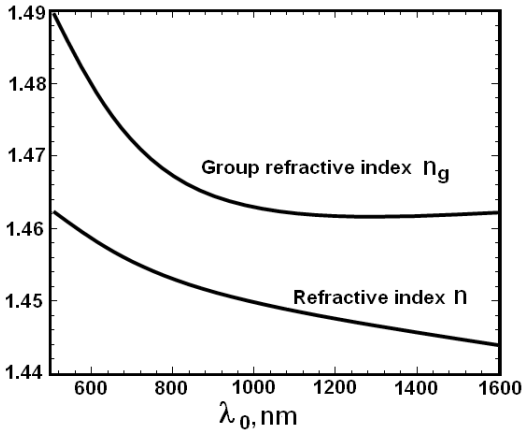

Figure 3.1: Group and phase refractive indices in bulk fused silica

Estimating the second derivative

The group velocity dispersion is described by $k_2 = (\lambda_0^3/2\pi c^2)\,(\partial^2 n/\partial \lambda^2)_{\lambda_0}$which is directly proportional to the dispersion parameter $D(\lambda_0) = -2\pi c k_2/\lambda_0^2$. It is possible to write

$$\left(\frac{\partial^2 n}{\partial \lambda^2} \right)_{\lambda_0} = -\frac{c}{\lambda_0} D(\lambda_0) \tag{3.2.4}$$

k_2 and $D(\lambda_0)$ are usually represented graphically in the bibliography.Thus, for example, for $\lambda_0 \approx 500$ nm one can estimate

$$\left| \frac{1}{2} \lambda_0^2 \left(\frac{\partial^2 n}{\partial \lambda^2} \right)_{\lambda_0} \right| = \frac{1}{2} |\lambda_0 c D(\lambda_0)| \leq 5 \times 10^{-2} \tag{3.2.5}$$

After these estimations, one has to simplify the Eq.3.2.2 and compare the terms. Multiplying Eq.3.2.2 by λ_0 and extracting the terms corresponding to the

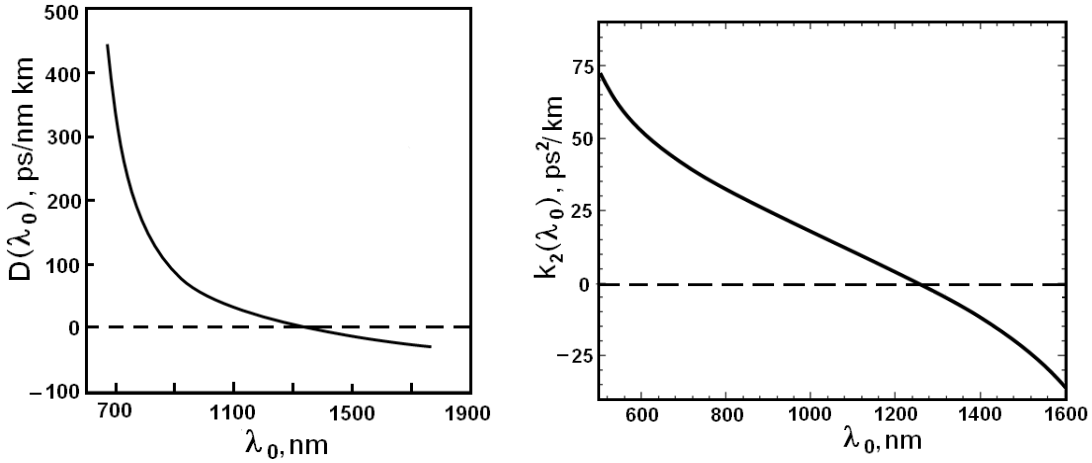

(a) (b)

Figure 3.2: Dispersion parameters in bulk fused silica

estimations from Eq.3.2.3 and 3.2.5

$$\begin{aligned}
&\lambda_0 \left(\frac{\partial n}{\partial \lambda}\right)_{\lambda_0} \frac{\Delta\lambda}{\lambda_0} + \frac{1}{2}\lambda_0^2 \left(\frac{\partial^2 n}{\partial \lambda^2}\right)_{\lambda_0} \frac{\Delta\lambda^2}{\lambda_0^2} - n(\lambda_0)\frac{\Delta\lambda}{\lambda_0} \\
&-\lambda_0 \left(\frac{\partial n}{\partial \lambda}\right)_{\lambda_0} \frac{\Delta\lambda^2}{\lambda_0^2} - \frac{1}{2}\lambda_0^2 \left(\frac{\partial^2 n}{\partial \lambda^2}\right)_{\lambda_0} \frac{\Delta\lambda^3}{\lambda_0^3} + n(\lambda_0)\frac{\Delta\lambda^2}{\lambda_0^2} \\
&+\lambda_0 \left(\frac{\partial n}{\partial \lambda}\right)_{\lambda_0} \frac{\Delta\lambda^3}{\lambda_0^3} + \frac{1}{2}\lambda_0^2 \left(\frac{\partial^2 n}{\partial \lambda^2}\right)_{\lambda_0} \frac{\Delta\lambda^4}{\lambda_0^4} = \frac{f\lambda_0}{V}
\end{aligned} \tag{3.2.6}$$

Equation 3.2.6 should be analyzed separately for two above-mentioned options. In the first case, of mutual independence $\Delta\lambda$ and f, it is possible to use the first approximation when the Eq. 3.2.6 could be simplified to

$$f = \frac{V}{\lambda_0}\left[\lambda_0 \left(\frac{\partial n}{\partial \lambda}\right)_{\lambda_0} - n(\lambda_0)\right]\left(\frac{\Delta\lambda}{\lambda_0}\right) \tag{3.2.7}$$

In the particular case of conventional codirectional collinear acousto-optical interaction in anisotropic medium, one could find $d\lambda \sim \Delta\lambda$ and $dn \sim \Delta n$ with $\Delta n \gg n(\lambda_0)|\Delta\lambda/\lambda_0|$, so that

$$f = \frac{V\Delta n}{\lambda_0} \tag{3.2.8}$$

In the second case of $\Delta\lambda = -c^{-1}\lambda_0^2 f$, one has to take into account the terms

being quadratic on $|\Delta\lambda/\lambda_0|$. This circumstance leads to the relation

$$\lambda_0 \left(\frac{\partial n}{\partial \lambda}\right)_{\lambda_0} \frac{\Delta\lambda}{\lambda_0} + \frac{1}{2}\lambda_0^2 \left(\frac{\partial^2 n}{\partial \lambda^2}\right)_{\lambda_0} \frac{\Delta\lambda^2}{\lambda_0^2} - n(\lambda_0)\frac{\Delta\lambda}{\lambda_0}$$
$$-\lambda_0 \left(\frac{\partial n}{\partial \lambda}\right)_{\lambda_0} \frac{\Delta\lambda^2}{\lambda_0^2} + n(\lambda_0)\frac{\Delta\lambda^2}{\lambda_0^2} = \frac{f\lambda_0}{V} \tag{3.2.9}$$

Simplifying the Eq.3.2.9 by the factor $\Delta\lambda = -c^{-1}\lambda_0^2 f$, one can obtain

$$f = \left(\frac{c}{\lambda_0}\right) \frac{\frac{c}{V} + n(\lambda_0) - \lambda_0 \left(\frac{\partial n}{\partial \lambda}\right)_{\lambda_0}}{n(\lambda_0) - \lambda_0 \left(\frac{\partial n}{\partial \lambda}\right)_{\lambda_0} + \frac{1}{2}\lambda_0^2 \left(\frac{\partial^2 n}{\partial \lambda^2}\right)_{\lambda_0}} \tag{3.2.10}$$

With $\lambda_0 \leq 10^{-4}$ cm for the visible range and $c = 3 \times 10^{10}$ cm/s, one can estimate $c/\lambda_0 \leq 3 \times 10^{14}$ Hz

3.3 Collinear AO interaction in a slightly dispersive uniaxial material

A set of stationary evolution equations for the amplitudes $C_0(x)$ and $C_1(x)$ of the incident and scattered light waves, respectively, with slightly mismatched wave vectors is given by [32, 33]

$$\frac{dC_{0,1}}{dx} = \mp\frac{q_{1,0}}{2} C_{1,0} \exp(\mp i\, \Delta k\, x), \tag{3.3.1}$$

$q_{0,1}$ are the amplitude parameters of the anomalous light scattering, $\Delta k = |\vec{k}_1 - \vec{k}_0 - \vec{K}|$ is the mismatch of wave vectors. Due to mismatch $\Delta k \neq 0$, the corresponding frequency bandwidth is

$$\Delta f \equiv \delta f = V\, L^{-1}, \tag{3.3.2}$$

L is the length of collinear interaction. Now, to take into account the linear acoustic losses and divergence of the acoustic beam in a crystalline material, it will be supposed that the parameters $q_{0,1}$ are now some functions of the coordinate x. The linear acoustic losses can be described, if there are setting $q_{0,1}(x) \propto \exp(-\alpha x)$,

where α is the amplitude factor of losses. The divergence of the acoustic beam can be characterized by the plane angle $\theta = \kappa\,\Lambda\,d \ll 1$, where the factor $\kappa \approx 1$, Λ is the acoustic wave lenght, and $d \gg \Lambda$ is the transducer aperture. The acoustic beam aperture $D(x)$ at the distance x can be estimated as $D(x) = d + \theta x$. The contribution of divergence looks like $q_{0,1}(x) \propto (1 - \beta x)^{-2}$, where $\beta = \theta/d$. To combine both these effects, $q_{0,1}(x) \propto q_{0,1}\exp(-\alpha x)(1 + \beta x)^{-2}$ will be taken and Eq. 3.3.1 will be modified as

$$\frac{dC_{0,1}}{dx} = \mp\frac{q_{1,0}}{2(1+\beta x)^2}\,C_{1,0}\,\exp[(-\alpha \mp i\,\Delta k)\,x], \tag{3.3.3}$$

with the conservation law in the form of $q_0|C_0|^2 + q_1|C_1|^2 = const$. Eqs. 3.3.3 should be solved with the boundary conditions

$$C_0(x=0) \;=\; A_0 \tag{3.3.4a}$$

$$C_1(x=0) \;=\; 0 \tag{3.3.4b}$$

where A_0 is the incident light amplitude. One can extract from Eq. 3.3.3 an individual stationary evolution equation for the scattered light wave

$$\frac{d^2C_1}{d^2x} + \frac{dC_1}{dx}\left(\frac{2\beta}{1+\beta x} + \alpha - i\,\Delta k\right) + \frac{q^2}{4}C_1(1+\beta x)^{-4}\exp(-2\alpha x) = 0, \tag{3.3.5}$$

where $q = \sqrt{q_0\,q_1} = \pi\lambda^{-1}\sqrt{2M_2\,P\,S_A}$ [32, 33], M_2 is the coefficient of acousto-optical merit inherent in a crystal, P is the acoustic power, and S_A is the initial cross-section area of acoustic beam close to the piezo-transducer. In the particular case of $\Delta k = 0$ and $A_0 = 1$, Eq. 3.3.5 has the following analytical solution

$$\begin{aligned} C_1(x) \;=\; \sin\Bigg\{ & \frac{q}{2\beta}\left[1 - \frac{e^{-\alpha x}}{1+\beta x}\right] + \frac{\alpha q}{2\beta^2}\exp\left(\frac{\alpha}{\beta}\right)\left[Ei\left(-\frac{\alpha}{\beta}\right)\right] \\ & -\frac{\alpha q}{2\beta^2}\exp\left(\frac{\alpha}{\beta}\right)\left[Ei\left(-\frac{\alpha}{\beta} - \alpha x\right)\right]\Bigg\} \end{aligned} \tag{3.3.6}$$

in terms of the exponential integral function $Ei(z)$

$$Ei(z) = -vp\int_{-z}^{\infty} t^{-1}e^{-t}dt$$

where the principal value of this integral is taken [34]. Equation 3.3.6 can be exploited to estimate the contributions of both the linear acoustic attenuation and the angular divergence to a collinear acousto-optical interaction. These two effects have different dependences on the acoustic frequency due to $\alpha \propto \Omega^2$ [35], while $\beta \propto 1/\Omega$. When $\Delta k \neq 0$ Eq. 3.3.5 can be exploited for estimating the effects of linear acoustic attenuation and angular divergence of the acoustic beam on the bandwidth of collinear interaction. For this purpose one can take $C_1(x) = A(x)\exp[i\varphi(x)]$, substitute it in Eq. 3.3.5 and obtain a set of two following equations

$$\frac{d^2A}{d^2x} + \frac{dA}{dx}\left(\frac{2\beta}{1+\beta x} + \alpha\right) + A\left\{\Delta k\frac{d\varphi}{dx} - \left(\frac{d\varphi}{dx}\right)^2 + \frac{q^2e^{-2\alpha x}}{4(1+\beta x)^4}\right\} = 0 \qquad (3.3.7)$$

$$A\frac{d\varphi}{dx} + \varphi\left[2\frac{dA}{dx} + A\left(\frac{2\beta}{1+\beta x} + \alpha\right)\right] - \Delta k\frac{dA}{dx} = 0 \qquad (3.3.8)$$

The equation 3.3.8 has the integral solution

$$\varphi(x) = A^{-2}(1+\beta x)^{-2}e^{-\alpha x}\left[\zeta + \frac{\Delta k}{2}\int\frac{d\left(A^2\right)}{dx}(1+\beta x)^2e^{\alpha x}dx\right] \qquad (3.3.9)$$

First, one can show that the integration constant ζ in Eq. 3.3.9 is perfectly inessential for the further consideration, so ζ can be taken to be zero. Second, it will be supposed that varying the last two terms under the integral in Eq. 3.3.9 is much slower than the first one and, consequently, these last terms can be factored out from the integral. After these two steps, Eq. 3.3.9 gives the approximate solution $\varphi(x) \approx \Delta k/2$ to Eq. 3.3.8, which corresponds to the case of neglecting the effects of linear attenuation and angular divergence on the acoustic beam in the phase $\varphi(x)$, i.e. of $\alpha = 0$ and $\beta = 0$.

Unfortunately, an exact solution to Eq. 3.3.7 can not be expresed in the closed analytical form even under the above-listed simplifications. That is why one are forced to make the third step in our approximations; namely, the Eq. 3.3.7 will be considered for the lowest approximation relative to the parameters α and β in each particular term. Such a strongly reduced form of Eq. 3.3.7 is given by

$$\frac{d^2A}{d^2x} + \frac{dA}{dx}(2\beta + \alpha) + \frac{A}{4}\left[(\Delta k)^2 + q^2\right] = 0 \qquad (3.3.10)$$

An exact solution to Eq. 3.3.10, with the natural boundary conditions, can be written as

$$A(x) \propto \exp\left[-\left(\frac{\alpha}{2}+\beta\right)x\right]\sin\left[\frac{x}{2}\sqrt{q^2+(\Delta k)^2-(\alpha+2\beta)^2}\right] \tag{3.3.11}$$

The bandwidth of scattering can be estimated by the first zero of a sinus function in Eq. 3.3.11, so one yield $L\sqrt{q^2+\Delta k^2-(\alpha+2\beta)^2}=2\pi$, therefore a small signal bandwidth with $q\to 0$ can be expressed as

$$\Delta f = V\sqrt{\frac{1}{L^2}+\frac{(\alpha+2\beta)^2}{4\pi^2}} \tag{3.3.12}$$

Δf is the corresponding frequency bandwidth. It should be noted that the contributions obtained in Eq. 3.3.12 for the considered effects are not additive to the portion listed in Eq. 3.3.2

3.4 Efficiency of collinear AO interaction in a calcium molybdate single crystal

Now, considering a few practically useful estimations related to experimental observation of the collinear acousto-optical interaction, with linear acoustic losses in a two-mode crystalline cell made of a calcium molybdate ($CaMoO_4$) single crystal, is possible to observe only anomalous process of light scattering, so that the parameters $q_{0,1}$ are described [32] by

$$q_{0,1} = \frac{\left|\vec{k}_{0,1}\right|}{4n_{0,1}^2}\left(\vec{\tilde{e}}_0\,\Delta\varepsilon\,\vec{e}_1\right) \tag{3.4.1}$$

$n_{0,1}$ are the refractive indices for the interacting light waves, $\left|\vec{k}_{0,1}\right| = 2\pi n_{0,1}/\lambda$, λ is the light wavelength in a vacuum, and the last term in brackets, describing the efficiency of interaction, is subject to find. This term includes the eigen-orts $\vec{e}_{0,1}$ of polarizations for the incident and scattered light beams as well as the tensor $\Delta\varepsilon$ of perturbations of the dielectric permittivity under action of the acoustic wave

in a medium. To estimate the efficiency of collinear acousto-optical interaction in a calcium molybdate cell, i.e. to find the contribution of brackets to Eq.3.4.1, it is necessary to find the dielectric permittivity perturbations tensor $\Delta\varepsilon$ whose components can be written as $\Delta\varepsilon_{ij} = \varepsilon_{im}\,\varepsilon_{nj}\,p_{mnkl}\,\gamma_{kl}$

The unperturbed dielectric permittivity tensor ε in the main crystallographic axes is

$$\varepsilon = \begin{pmatrix} \varepsilon_0 & 0 & 0 \\ 0 & \varepsilon_0 & 0 \\ 0 & 0 & \varepsilon_e \end{pmatrix} \tag{3.4.2}$$

$\varepsilon_0 = n_0^2$ and $\varepsilon_e = n_e^2$ are the eigen-values of the unperturbed dielectric permittivity tensor ε.

Using the same procedure like in section 2.2.2 and taking the photoelastic tensor p (see section 2.3.1) of the fourth rank for a calcium molybdate single crystal in the form of a 6×6 matrix $\hat{p}$, it will be allowed first to construct and to calculate the product $\hat{p}\bar{\gamma} = \gamma_0(0, 0, 0, p_{45}, p_{44}, 0)$, and then to convert the result back to the form of a standard tensor $(p\gamma)$ of the second rank. Then, the result of calculating has the form

$$\Delta\varepsilon = \gamma_0\,\varepsilon_0\,\varepsilon_e \begin{pmatrix} 0 & 0 & p_{44} \\ 0 & 0 & p_{45} \\ p_{44} & p_{45} & 0 \end{pmatrix} \tag{3.4.3}$$

Now, taking into account the orts (unit vectors) $\vec{e}_{0,1}$ of polarization for the incident and scattered light waves. When the wave vectors of these light waves are collinear to both the wave normal ort $\vec{m}$, for the acoustic wave, and to the [100] -axis in calcium molybdate crystal, the eigen-orts $\vec{e}_{0,1}$ of light polarizations should be oriented along the [0,1,0] and [0,0,1] axes [see Eq. 3.4.2], so that one can take for example $\vec{e}_0 = [0, 1, 0]$ and $\vec{e}_1 = [0, 0, 1]$ with $n_0 = n_o$ and $n_1 = n_e$. And it is obtained the contribution of the brackets in Eq. 3.4.1

$$\vec{\tilde{e}}_0\,\Delta\varepsilon\,\vec{e}_1 = \vec{\tilde{e}}_1\,\Delta\varepsilon\,\vec{e}_0 = \gamma_0\,\varepsilon_0\,\varepsilon_e\,p_{45} \tag{3.4.4}$$

In so doing, it is possible to find that $q_{0,1} = \pi(2\lambda)^{-1} n_{e,o} \gamma_0 n_{o,e}^2 p_{4,5}$. The difference beetwen q_0 and q_1 is rather small, because $q_o/q_1 = n_o/n_e$. Due to the amplitude of deformation can be explained as

$$\gamma_0 = \sqrt{\frac{2P}{\rho V^3}}$$

one can finally obtain

$$q_0 = \frac{\pi}{\lambda}\sqrt{\frac{P}{2}\left(\frac{n_e^2 n_o^4 p_{45}^2}{\rho V^3}\right)} \tag{3.4.5a}$$

$$q_1 = \frac{\pi}{\lambda}\sqrt{\frac{P}{2}\left(\frac{n_o^2 n_e^4 p_{45}^2}{\rho V^3}\right)} \tag{3.4.5b}$$

P is the acoustic power density. The factors taken in brackets in Eqs. 3.4.5 represent the acousto-optical figures of merit M_2 peculiar for estimating the efficiency of crystalline materials in acousto-optics [36].

Numerical estimations

At this step, it is possible to perform a few numerical estimations. First, the acousto-optical figures of merit M_2, peculiar to the geometry of collinear interaction under consideration, will be estimated. The magnitude of M_2 depends pricipally on the constant p, which can vary over a wide range from crystal to crystal. Suffiently effective collinear scattering of light by bulk acoustic wave associated with $|p| \geq 0.05$, had been observed in cell made of the three following single crystals: quartz (α-SiO_2) and lithium niobate ($LiNbO_3$) on the longitudinal acoustic waves passing along the x-axis and on the shear waves running along y-axis, and then, calcium molybdate ($CaMoO_4$) on the shear wave passing along the x-axis. Among these crystals, collinear interaction on the shear acoustic wave in calcium molybdate with $p = p_{45} = 0.06$ exhibits the lowest frecuency Ω lying in a frequency range of about $30 - 100$MHz for light beams in visible range of spectrum. The other parameters are: $\rho = 4.34\text{g/cm}^3$ and $V = 2.95 \times 10^5\text{cm/s}$, while the refractive indices are slightly dispersive in behavior (see Table 3.4.1) [37].

Taking, for example, $p_{45} = 0.06$, $n_e = 2.0239$, and $n_o = 2.0116$ at the chosen light wavelength 532nm [38, 39] and calculate $M_2 \approx 2.07 \times 10^{-18}\mathrm{s}^3/\mathrm{g}$ in a quite acceptable approximation of $q_0 \approx q_1$, i.e. with an accuracy of about 1%. Then the dependence of the acoustic frequency f on the light wavelength λ can be found from Eq. 3.2.8 and Table 3.4.1. For instance, the magnitude of this frequency can be estimated as $f \approx 61\mathrm{MHz}$ at the green light wavelength λ of 532nm. Then, the parameter of linear acoustic losses for the shear acoustic waves passing along the x-axis is about $\Gamma = 60\mathrm{dB}/(\mathrm{cm\ GHz}^2)$, that gives us, for example, the above-introduced amplitude factor of acoustic attenuation $\alpha = (\ln 10/20)\Gamma f^2 \approx 0.025\mathrm{cm}^{-1}$ at the frequency of 61MHz. The angular divergence of acoustic beam in a calcium molybdate collinear cell at the frequency $f = 61\mathrm{MHz}$ can be estimated as well. Practically, a realiable spatial size of the initial acoustic beam aperture, which will be consider, is close to $d \approx 0.3$ cm. Thus one can estimate $\Lambda = V/f = 4.82 \times 10^{-3}\mathrm{cm}$, $\beta = \Lambda/d^2 = 5.35 \times 10^{-2}\mathrm{cm}^{-1}$ and conclude that α and β have the same order of magnitudes in the particular case of calcium molybdate under consideration.

λ (nm)	500	600	700	800	900	1000
n_e	2.0239	1.9983	1.9843	1.9781	1.9705	1.9658
n_o	2.0116	1.9884	1.9775	1.9683	1.9634	1.9597

Table 3.4.1: Dispersion of the main refractive indices n_e and n_o in the calcium molybdate single crystal [38, 39]

3.5 Scheme for the experiments within a calcium molybdate cell

To realize experimentally the process of acousto-optic filtering, it will be used the schematic arrangement depicted in Fig. 3.3. It consists of a continuous-wave

laser, a crystalline acousto-optical cell with a pair of polarizers, whose combinated scheme is presented in details on Fig. 3.4, a photo-detector, and a set of electronic equipment for generating and registering the corresponding electric ultra-high-frequency (UHF) radio-wave signal, which is applied to the electronic input of the collinear acousto-optical cell (see Fig. 3.4) and to the oscilloscope as the etalon signal (see Fig. 3.3). A two-mode copropagating collinear $CaMoO_4$ crystalline cell was characterized by a crystal length $L = 44$mm along the [100]-axis, and an acoustic velocity $V = 2.95 \times 10^5$ cm/s for the shear elastic mode, whose displacement vector is oriented along the [001]-axis.

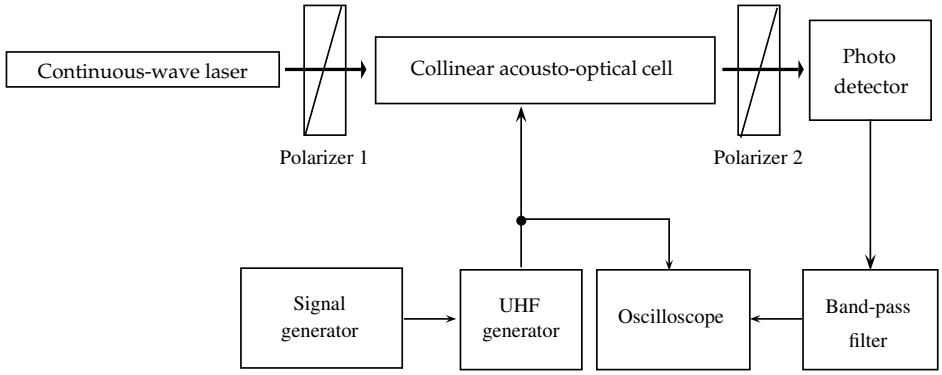

Figure 3.3: Schematic arrangment of the experimental set-up

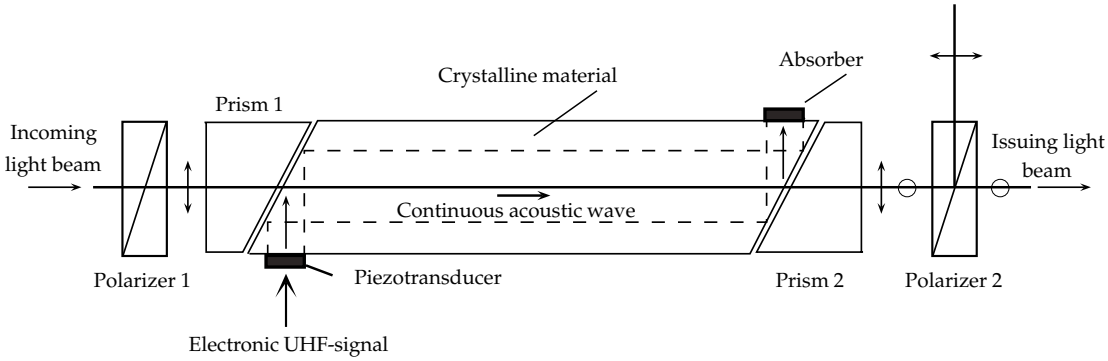

Figure 3.4: Scheme of the copropagating collinear calcium molybdate acousto-optical cell providing the traveling-wave regime of interaction

The continuous-wave beam at a green light wavelength $\lambda = 532$nm was used as an optical pump during the experiments. The first polarizer was precisely

aligned in correspondence with the optical axes of a crystal in the cell. After the interaction with an acoustic signal, already two ortogonally polarized light beams, incident and signal ones, passed through the cell. The second polarizer gave an opportunity to be aligned in correspondence with the polarization of the signal beam and to extract the output optical signal.

3.6 Conclusions

The obtained experimental data make possible considering a few estimations of an advanced collinear AOF based on calcium molybdate single-crystal. This new AOF with a 15-microsecond time-aperture operates over all the visible range exhibiting 60%-efficiency at the electric power 1.0 W. Its bandwidth, which in fact characterizes the resolution due to the well-known relation $\Delta f \equiv \delta f$ between the frequency bandwidth and the frequency resolution in the case of collinear scheme, includes two contributions. The first one does not depend on the divergence angles of both optical an acoustic beams, and it prevails when these angles are under a critical angle.

The second contribution dominates with really wide-angle divergence of these beams or when AOF crystal is sufficiently long; so that the bandwidth shows a quadratic growth as the divergence angles increase. Estimating that critical angle shows that it does not exceed 10 degres when the crystal is shorter than 6 cm in length and the acoustic frequency is lower than 100 MHz.

Chapter 4

Acousto-optical spectrum analysis of radio-wave signals using collinear wave heterodyning

4.1 Introduction

The technique under proposal for a precise spectrum analysis within an algorithm of the collinear wave heterodyning implies a two-stage integrated processing, namely, the wave heterodyning of a signal in a square-law nonlinear medium and then the optical processing in the same solid state cell. Technical advantage of this approach lies in providing a direct multichannel parallel processing of ultrahigh-frequency radio-wave signals with essentially improved frequency resolution.

Analytic expression for the corresponding effective acoustic modulus of the third order in KRS-5 has been found. Contrary to the recently developed theoretical approach based on the technique of substantial approximations [8, 9], a regime of the coupled acoustic modes is considered, which provides more accurate analysis.

4.2 Efficiency of acousto-optical interaction in a KRS-5 cubic single crystal

One can start from estimating the potential efficiency I of Bragg light scattering by the longitudinal acoustic waves in a KRS-5 single crystal. Taking the same orientation shown in Fig. 4.1. To obtain the figure of acousto-optical merit M_2 inherent in the selected cut of a KRS-5 crystal, first of all both the effective photo-elastic constant $p_{eff} = \vec{e_1}(p\gamma^{(L)})\vec{e_0}$ and the velocity V_L must be found. Taking into account the result in eq. 2.2.4 and the photoelastic tensor in 2.3.2, one can calculate the matrix product $p\bar{\gamma}^{(L)} = (1/3)(p_{11} + 2p_{12}, p_{11} + 2p_{12}, p_{11} + 2p_{12}, 2p_{44}, 2p_{44}, 2p_{44})$ and convert it back to the form of a standard tensor ($p\,\gamma^{(L)}$) of the second rank [14]. The effective photo-elastic constant can be written from the scalar form

$$p_{eff} = \frac{1}{3}\vec{e_1}\begin{pmatrix} p_{11}+2p_{12} & 2p_{44} & 2p_{44} \\ 2p_{44} & p_{11}+2p_{12} & 2p_{44} \\ 2p_{44} & 2p_{44} & p_{11}+2p_{12} \end{pmatrix}\vec{e_0} \qquad (4.2.1)$$

$\vec{e_0}$ and $\vec{e_1}$ describe the polarization states of incident and scattered light beams, respectively.

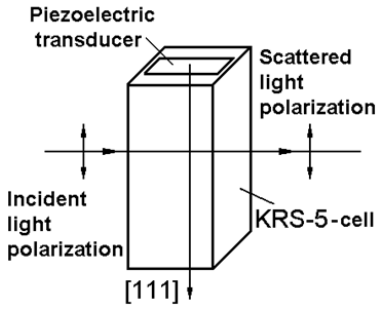

Figure 4.1: Crystallographic orientations for the piezoelectric transducer and the crystalline material in a KRS-5 cell.

Due to $\vec{K}||[111]$, if the Bragg angles are omitted as small values, the wave vectors $\vec{k_0}$ and $\vec{k_1}$ of the incident and scattered light beams, respectively, should

lie in the (111)-plane to be orthogonal to $\vec{K}$]. One can put $\vec{k}_0 = \vec{k}_1 = \vec{k}$ when the Bragg angles are neglected. Due to optical isotropy of cubic KRS-5 crystal, one can select $\vec{k}||[1\bar{1}0]$. In this particular case, one has an opportunity to consider the vectors $\vec{e}_0$ and $\vec{e}_1$ belonging to $(1\bar{1}0)$-plane, which includes [110], [111] and [001] axes; therewith the axes [110] and [001] give an orthogonal basis, because $[110]\perp[001]$. In so doing, one takes at first the angles $\alpha_{0\,,1}$ as current angles between $\vec{e}_{0\,,1}$ and the [001]-axis. Consequently, one can easily obtain that $\vec{e}_{0,1} = \Big(\sin\alpha_{0,1}/\sqrt{2}, \sin\alpha_{0,1}/\sqrt{2}, \cos\alpha_{0,1}\Big)$, so that $\vec{e}_{0,1}||[001]$ when $\alpha_{0,1} = 0$. Changing the initial position for the vectors $\vec{e}_{0,1}$ via the substitution the angles $\alpha_{0,1}$ by the new angles $\alpha_{0,1} + \beta_1$, where $\beta_1 = \arccos(1/\sqrt{3})$; i.e. one can write

$$\vec{e}_{0,1} = \left(\frac{1}{\sqrt{2}}\sin(\alpha_{0,1}+\beta_1),\ \ \frac{1}{\sqrt{2}}\sin(\alpha_{0,1}+\beta_1),\ \ \cos(\alpha_{0,1}+\beta_1)\right) \tag{4.2.2}$$

After such a substitution, one will have finally obtained that $\vec{e}_{0,1}||[111]$ when $\alpha_{0,1} = 0$. Usually, two types of light scattering can be realized. At first, one can consider the normal scattering when $\alpha_1 = \alpha_0$. In this case,

$$\begin{aligned} p_{eff}^{(n)} \ &= \ \frac{1}{3}\Big\{(p_{11}+2p_{12}+2p_{44})\sin^2(\alpha_0+\beta_1) + 2\sqrt{2}p_{44} \\ &\quad \times \sin[2(\alpha_0+\beta_1)] + (p_{11}+2p_{12})\cos^2(\alpha_0+\beta_1)\Big\} \end{aligned} \tag{4.2.3}$$

Eq. 4.2.3 was simulated numerically with $p_{11} = 0.21$, $p_{12} = 0.22$, and $p_{44} = 0.15$ (see Fig. 4.2(a)). The oscillating plot exhibits a maximum magnitude $p_{eff\,\max}^{(n)} = 0.417$ at $\alpha_0 = \pi k$, $k = \{\cdots, -1, 0, 1, \cdots\}$ and a minimum magnitude $p_{eff\,\min}^{(n)} = 0.117$ at $\alpha_0 = (\pi/2) + \pi k$. The second type is associated with the anomalous light scattering when $\alpha_1 = \alpha_0 + (\pi/2)$. Similar process is characterized by

$$p_{eff}^{(an)} = \frac{p_{44}}{3}\Big\{\sin[2(\alpha_0+\beta_1)] + 2\sqrt{2}\cos[2(\alpha_0+\beta_1)]\Big\} \tag{4.2.4}$$

This value reaches its maxima $p_{eff\,max}^{(an)} = 0.15$ with $\alpha_0 = (\pi/4) + (\pi k/2)$. The plots associated with these angular distributions for the effective photo-elastic constants in a KRS-5 single crystal are shown in Fig. 4.2(b).

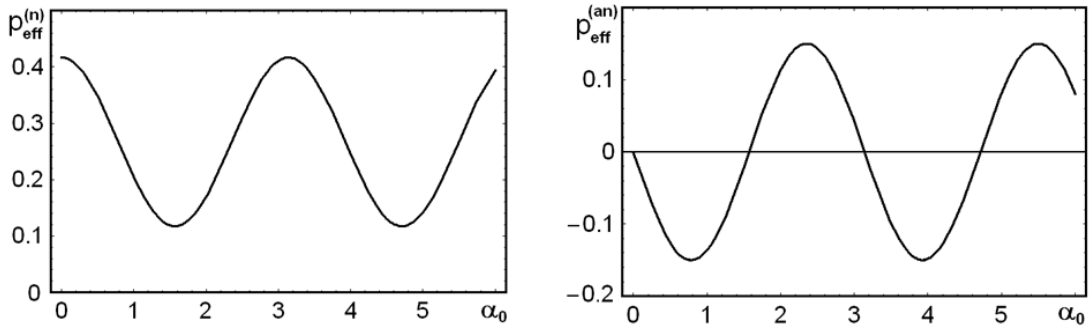

(a) (b)

Figure 4.2: Abolute dependences for the effective photo-elastic constants in a KRS-5 single crystal versus the angle α_0: normal light scattering (a) and anomalous light scattering (b)

One can use the tensor C of elastic moduli to estimate the velocity of the longitudinal wave. Its components $C_{\lambda\mu}$ will be non-zero only with $C_{11} = C_{22} = C_{33}$, $C_{44} = C_{55} = C_{66}$, and $C_{12} = C_{13} = C_{21} = C_{23} = C_{31} = C_{32}$. The corresponding effective elastic modulus of the second order is

$$C_2 = (1/3)(C_{11} + 2C_{12} + 4C_{44}) \tag{4.2.5}$$

which describes the velocity V_L inherent in the selected pure elastic longitudinal mode as $V_L = \sqrt{C_2/\rho}$, where ρ is the material density. Using $C_{11} = 3.4 \cdot 10^{11}$ dyne/cm^2, $C_{12} = 1.3 \cdot 10^{11}$ dyne/cm^2, $C_{44} = 0.58 \cdot 10^{11}$ dyne/cm^2, and $\rho = 7.37$ g/cm^3 peculiar to a KRS-5 crystal and estimate $V_L = 1.92 \cdot 10^5$ cm/s. Together with this, one has to note that acoustic attenuation peculiar to this acoustic mode is not too low and is characterized by the factor $\Gamma = 10$ dB/(cm GHz^2) [38, 39].

The maximal magnitude inherent in the corresponding figures of acousto-optical merit, $M_2 = n^6 \left(p^{(n)}_{eff\,max}\right)^2/(\rho V_L^3) \approx 930 \times 10^{-18}$ s^3/g with $n = 2.57$ at $\lambda = 671$ nm, is related to the normal scattering in a KRS-5 single crystal. The performed calculations demonstrate that the normal light scattering by the longitudinal elastic wave is a few times more efficient than the anomalous one.

The other side of estimating the efficiency of acousto-optic interaction is con-

nected with choosing the regime of light scattering. The most efficient one is the Bragg regime, which is shown in fact in Fig.4.3(a). It allows a 100% efficiency of light scattering and occurs with large enough length L of interaction between light and acoustic waves when the dynamic acoustic diffractive grating is sufficiently thick.

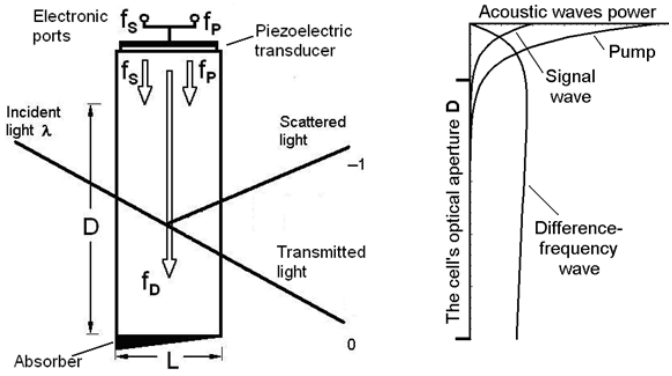

(a) (b)

Figure 4.3: Schematic arrangment of the interacting beams in a two-cascade acousto-optical cell (a), and the illustrating spatial distribution for powers of the interacting acoustics waves (b).

Such a regime can be realized only when the angle of light incidence on that acoustic grating meets the corresponding Bragg condition, which can be assumed to be provided in advance, and the inequality $Q = 2\pi\lambda L f_D^2/(n\,V_L^2) >> 1$ for the Klein-Cook factor Q [30] is satisfied.

Taking, for example, $\lambda = 671$nm, $L = 1.0$ cm, and $V_L = 1.92 \times 10^5$ cm/s, one can estimate $Q \geqslant 7$ for $f_D > 40$MHz. Thus, the Bragg regime of light scattering could be expected for the acoustic difference-frequencies at least exceeding 40MHz in a KRS-5 single crystal, so that the acoustic frequency $f_D = 40$MHz can be considered as a lower limit for the Bragg regime of light scattering.

4.3 Codirectional collinear acoustic wave heterodyning

At this stage, effect of a three-acoustic wave mixing associated with the longitudinal elastic wave propagating along the [111]-axis in a KRS-5 single crystal is under consideration. It can be done using the Shapiro-Thurston equation [40] reduced down to terms of the third order in its general form

$$\rho\frac{\partial^2 u_i}{\partial t^2} - C_{ijkl}\frac{\partial^2 u_k}{\partial x_j \partial x_l} = \tilde{C}_{ijklqr}\frac{\partial u_q}{\partial x_r}\frac{\partial^2 u_k}{\partial x_j \partial x_l} \tag{4.3.1}$$

$$\tilde{C}_{ijklqr} = C_{ijklqr} + C_{ijlq}\delta_{kr} + C_{ilqr}\delta_{jk} + C_{iklq}\delta_{jr} \tag{4.3.2}$$

These equations include all the components. In the above-chosen configuration, the direction cosines $n_i\,(i = 1, 2, 3)$ should satisfy a pair of the following obvious conditions $n_1 = n_2 = n_3$ and $n_1^2 + n_2^2 + n_3^2 = 1$, so that $n_i = 1\big/\sqrt{3}$. Using Eqs.4.3.1, 4.3.2, and after some calculations, one can obtain the following effective elastic modulus of the third order

$$C_3 = C_{111}+2C_{123}+6C_{112}+12C_{144}+16C_{456}+24C_{155}+9C_{11}+18C_{12}+36C_{44} \tag{4.3.3}$$

and (exploiting, for example, the data from Ref. [41]) conclude that the longitudinal elastic wave propagating along the [111]-axis is definitely capable of mixing the acoustic waves in a KRS - 5 single crystal.

Now, one can introduce the new coordinate axis x oriented along the [111] crystallographic axis of KRS-5, so that $\vec{x}||\vec{m}||[111]$ and Eq.4.3.1 takes the form

$$\frac{\partial^2 u}{\partial t^2} - V_L^2\,\frac{\partial^2 u}{\partial x^2} = \frac{C_3}{\rho}\;\frac{\partial u}{\partial x}\;\frac{\partial^2 u}{\partial x^2} \tag{4.3.4}$$

The first term in Eq.4.3.4 can be approximately converted within the quasi-linear linear form of $\partial u/\partial t \approx -V_L(\partial u/\partial x)$ as $\partial^2 u/\partial t^2 \approx -V_L(\partial^2 u/\partial x\,\partial t)$. Then, using the obvious relation $2\,(\partial u/\partial x)\,(\partial^2 u/\partial x^2) = (\partial/\partial x)(\partial u/\partial x)^2$, one

can integrate Eq. 4.3.4 with respect to x. After that an additional phenomenological term $\alpha\, V_L\, u$ can be included to take into account linear acoustic losses, which are physically characterized by the amplitude decrement α , reflecting usually just the square-law frequency dispersion of losses in solids. As a result, one can write

$$\frac{\partial\, u}{\partial\, t} + V_L\, \frac{\partial\, u}{\partial\, x} + \alpha\, V_L\, u = \frac{\Gamma}{2}\, V_L\, \left(\frac{\partial\, u}{\partial\, x}\right)^2 \tag{4.3.5}$$

where $\Gamma = -\, C_3 / C_2, V_L = \sqrt{C_2/\rho}$, and $C_2 = (\, C_{11} + 2\, C_{12} + 4\, C_{44}\,)/3$ is the elastic modulus of the second order for $\vec{x}||\vec{m}||[111]$. A one-dimensional wave equation [Eq. 4.3.5] for the complex amplitude of an elastic wave is peculiar for characterizing a three-wave mixing in a medium with linear dispersive losses and square-law nonlinearity. Because of a square-law dispersion of acoustic losses, the complex amplitude u can be taken in the form of a superposition of only a triplet of waves including the pump, the signal wave, and the difference-frequency wave, namely, $u = u_P + u_S + u_D$, while the second harmonics of both the pump and the signal wave as well as their sum-frequency component can be omitted in this project of the chosen solution. Starting, for example, from the pump, one can write the corresponding complex amplitude as $u_P\,(\,x\,,\,t\,) = A_P\,(\,x\,)\ \exp\,[\,i\,(\,k_P\,x - \omega_P\,t\,)\,] + A_P^*\,(\,x\,)\ \exp\,[\,-\,i\,(\,k_P\,x - \omega_P\,t\,)\,]$ and note its losses as α_P. Substituting this formula into the left hand side of Eq. 4.3.5, one can calculate

$$\begin{aligned} V_L^{-\,1}\, \frac{\partial\, u_P}{\partial\, t} + \frac{\partial\, u_P}{\partial\, x} + \alpha_P\, u = {} & \left[\alpha_P\, A_P + \frac{d\, A_P}{d\, x}\right]\ \exp\,[\,i\,(\,k_P x - \omega_P t\,)\,] + \\ & \left[\alpha_P\, A_P^* + \frac{d\, A_P^*}{d\, x}\right]\ \exp\,[\,-\,i\,(\,k_P x - \omega_P t\,)\,] \end{aligned} \tag{4.3.6}$$

It is seen that the relations analogous to Eq.4.3.6 can be obtained for the signal and difference-frequency waves. To construct the contribution $(\partial\, u/\partial\, x)^2$ in the right hand side of Eq.4.3.5 one has to estimate the summands. Applying the slowly varying amplitudes technique, one has to take into account the inequalities $|\, d\, A_j\,(\,x\,)/d\, x\,| \ << \ k_j\ |\, A_j\,(\,x\,)\,|,\ j \in [\,P,\, S,\, D\,]$. Consequently, the following

approximation appears

$$\left(\frac{\partial u}{\partial x}\right)^2 \approx \quad (ik_P\{A_P(x)\exp[i(k_Px-\omega_Pt)]-A_P^*(x)\exp[-i(k_Px-\omega_Pt)]\} + ik_S\{A_S(x)\exp[i(k_Sx-\omega_St)]-A_S^*(x)\exp[-i(k_Sx-\omega_St)]\} + ik_D\{A_D(x)\exp[i(k_Dx-\omega_Dt)]-A_D^*(x)\exp[-i(k_Dx-\omega_Dt)]\})^2 \tag{4.3.7}$$

Now, one must consider two different regimes of a three-wave mixing. The right hand sides of Eqs.4.3.6 and 4.3.7 give

1. $f_S = f_P + f_D$:

$$\frac{dA_S}{dx}+\alpha_S A_S = \beta_S A_D A_P \tag{4.3.8a}$$
$$\frac{dA_P}{dx}+\alpha_P A_P = -\beta_P A_D^* A_S \tag{4.3.8b}$$
$$\frac{dA_D}{dx}+\alpha_D A_D = -\beta_D A_P^* A_S \tag{4.3.8c}$$

2. $f_P = f_S + f_D$:

$$\frac{dA_P}{dx}+\alpha_P A_P = \beta_P A_D A_S \tag{4.3.9a}$$
$$\frac{dA_S}{dx}+\alpha_S A_S = -\beta_S A_D^* A_P \tag{4.3.9b}$$
$$\frac{dA_D}{dx}+\alpha_D A_D = -\beta_D A_S^* A_P \tag{4.3.9c}$$

where $\beta_S = 0.5\,\Gamma\,k_P k_D$, $\beta_P = 0.5\,\Gamma\,k_S k_D$, and $\beta_D = 0.5\,\Gamma\,k_P k_S$ are the coupling factors. At this step, one can take $A_{D,S,P} = a_{D,S,P}\,\exp\,[\,i\,(\,\varphi_{D,S,P}\,)\,]$, where $a_{D,S,P}$ and $\varphi_{D,S,P}$ are the real-valued amplitudes and phases of non-optical waves. Consider, for example, Eq. 4.3.8 governing the system in a regime of $f_S = f_P + f_D$ with sign$(\,f_P - f_S\,) = -1$. Dividing real and imaginary parts in Eq. 4.3.8, one can find two groups of the real-valued equations

$$\frac{da_S}{dx}+\alpha_S a_S = \beta_S a_D a_P\,\cos\,(\,\varphi_S-\varphi_D-\varphi_P\,) \tag{4.3.10a}$$
$$\frac{da_D}{dx}+\alpha_D a_D = -\beta_D a_S a_P\,\cos\,(\,\varphi_S-\varphi_D-\varphi_P\,) \tag{4.3.10b}$$
$$\frac{da_P}{dx}+\alpha_P a_P = -\beta_P a_D a_S\,\cos\,(\,\varphi_S-\varphi_D-\varphi_P\,) \tag{4.3.10c}$$

$$\frac{d\,\varphi_S}{dx} a_S = \beta_S\, a_D\, a_P\ \sin\,(\,\varphi_S - \varphi_D - \varphi_P\,) \tag{4.3.11a}$$

$$\frac{d\,\varphi_D}{dx}\, a_D = -\,\beta_D\, a_S\, a_P\ \sin\,(\,\varphi_S - \varphi_D - \varphi_P\,) \tag{4.3.11b}$$

$$\frac{d\,\varphi_P}{dx}\, a_P = -\,\beta_P\, a_D\, a_S\ \sin\,(\,\varphi_S - \varphi_D - \varphi_P\,) \tag{4.3.11c}$$

Equations 4.3.10 and 4.3.11 can be analyzed with the natural for similar problems boundary conditions $U_P \neq 0$, $U_S \neq 0$, and $U_D = 0$, where $U_{P,S,D} = A_{P,S,D}\,(x = 0)$. With these conditions, one can find from Eq.4.3.10b that $\frac{da_D}{dx}\ (x = 0\,) = -\ \beta_D\, U_P\, U_S$. Here, the following quite natural approximation can be done; namely, putting $a_P >> a_S,\ a_D$ almost everywhere in an area of interaction. In this particular case, Eq.4.3.10c can be solved in a given field approximation as $a_P = U_P\ \exp\,(\,-\alpha_P\, x\,)$, while Eq.4.3.11c gives $\frac{d\,\varphi_P}{dx} = 0$. Substituting these solutions into Eqs.4.3.10 and 4.3.11 and dividing real and imaginary parts, one can obtain

$$\frac{d\,a_S}{dx} + \alpha_S\, a_S = \beta_S\, a_D\, U_P\ \exp\,(\,-\alpha_P\, x\,)\ \cos\ \varphi \tag{4.3.12a}$$

$$\frac{d\,a_D}{dx} + \alpha_D\, a_D = -\,\beta_D\, a_S\, U_P\ \exp\,(\,-\alpha_P\, x\,)\ \cos\ \varphi \tag{4.3.12b}$$

$$\frac{d\,\varphi}{dx} = U_P\ \exp\,(\,-\alpha_P\, x\,)\ \sin\,\varphi\ \left(\beta_D\,\frac{a_S}{a_D} - \beta_S\,\frac{a_D}{a_S}\right) \tag{4.3.12c}$$

$$\varphi = \varphi_S - \varphi_P - \varphi_D \tag{4.3.12d}$$

From the first integral of Eqs.4.3.12, with allowance for the boundary condition $a_D\,(x = 0) = 0$, which is characteristic of wave heterodyning, one can find that $d\varphi/dx \equiv 0$ and $\sin\,\varphi \equiv 0$, so that one can take, for example, $\cos\ varphi = 1$. Equations 4.3.9a-4.3.9c, associated with the regime $f_P = f_S + f_D$ with $\mathrm{sign}(\,f_P - f_S\,) = +1$, can be analyzed by similar way via substituting $\beta_S \to -\,\beta_S$. Consequently, Eqs.4.3.12a and 4.3.12b give the two following pairs of the combined ordinary differential equations of the first order

$$\frac{d\,a_S}{dx} + \alpha_S\, a_S = -\ \mathrm{sign}\,(\,f_P - f_S\,)\,\beta_S\, a_D\, U_P\ \exp\,(\,-\alpha_P\, x\,) \tag{4.3.13a}$$

$$\frac{d\,a_D}{dx} + \alpha_D\, a_D = -\,\beta_D\, a_S\, U_P\ \exp\,(\,-\alpha_P\, x\,) \tag{4.3.13b}$$

Excluding a_S from Eq. 4.3.13, one can write a linearized version for the needed second-order ordinary differential equation

$$\frac{d^2a_D}{dx^2} + (\alpha_P + \alpha_S + \alpha_D)\frac{da_D}{dx} + [\alpha_D(\alpha_P + \alpha_S) - \text{sign}(f_P - f_S)\beta_S\beta_D U_P^2 \exp(-2\alpha_P x)\Big]\, a_D = 0 \tag{4.3.14}$$

Because of the above-mentioned dispersion of losses included in the factors α_P, α_S and α_D, one can extract their square-law proportionalities to the corresponding carrier frequencies of acoustic waves $\alpha_{P,S,D} \sim f^2_{P,S,,D}$ and write

$$\alpha_P + \alpha_S + \alpha_D = 2\,\alpha_P\,[\,1 + \delta\ \text{sign}\,(\,f_P - f_S\,) + \delta^2\,] \tag{4.3.15a}$$

$$\alpha_P + \alpha_S - \alpha_D = 2\,\alpha_P\,[\,1 + \delta\ \text{sign}\,(\,f_P - f_S\,)\,] \tag{4.3.15b}$$

with $\delta = f_D/f_P << 1$. Introducing the notations $g = -\,\delta\ \text{sign}\,(\,f_P - f_S\,) + \delta^2$, and $h = \delta\ \ \text{sign}\,(\,f_P - f_S\,)$, so that $g \approx -\,h$ due to the smallness of δ, one can express the exact solution to Eq.4.3.14 in terms of the Bessel functions as

$$\begin{aligned} a_D\,(x) \;\; = \;\; & \exp\,[-\alpha_P x(1+g)]\,\Big\{C_1 Z_{(h-1)}\,[\xi\exp\,(-\alpha_P x)] \\ & + C_2 Z_{(1-h)}\,[\xi\exp\,(-\alpha_P x)]\Big\} \end{aligned} \tag{4.3.16}$$

where $\xi = \alpha_P^{-1}\,U_P\,\sqrt{\beta_S\,\beta_D}$, is the normalized acoustic wave amplitude. Then, $Z_\nu = J_\nu$ when $f_P <\ \ f_S$ and sign$(\,f_P - f_S\,) = -1$, while $Z_\nu = I_\nu$ with $f_P > f_S$ and sign$(\,f_P - f_S\,) = +1$ (for example, see Ref. [42]). J_ν and I_ν are the first and second orders Bessel, respectively. Exploiting the above-mentioned boundary conditions for a_D and its spatial derivative, one can determine the constants $C_{1\,,\,2}$ of integration in Eq.4.3.16 as

$$C_1 = \left(\frac{-\,2\ \beta_D\,U_P\,U_S}{\alpha_P\,\xi}\right)\ \frac{Z_{(\,1-h)}\,(\,\xi\,)}{W\,(\,\xi\,,\,h\,)} \tag{4.3.17a}$$

$$C_2 = \left(\frac{2\ \beta_D\,U_P\,U_S}{\alpha_P\,\xi}\right)\ \frac{Z_{(\,h-1)}\,(\,\xi\,)}{W\,(\,\xi\,,\,h\,)} \tag{4.3.17b}$$

$$\begin{aligned} W\,(\,\xi\,,\,h\,) = {} & Z_{(1-h)}(\,\xi\,)\,[Z_{(\,h-2)}(\,\xi\,) + \text{sign}(f_P - f_S)Z_h(\,\xi\,)] \\ & - Z_{(h-1)}(\,\xi\,)\,[Z_{(\,-h)}(\,\xi\,) + \text{sign}(f_P - f_S)Z_{(2-h)}(\,\xi\,)] \end{aligned} \tag{4.3.18}$$

Thus, Eqs.4.3.16 - 4.3.18 represent the solution describing the spatial distribution for the difference-frequency acoustic wave along the acousto-optical cell exploiting collinear acoustic wave heterodyning. In the above-noted particular cases, Eq.4.3.18 can be simplified as $W\,(\,\xi\,,\,h\,) = -\,4\,(\,\pi\,\xi\,)^{-1}\,\sin\,(\,\pi\,\delta\,)\,\,\mathrm{sign}\,(\,f_P - f_S\,)$, so that one can write

1. $f_S = f_P + f_D$, $\mathrm{sign}(f_P - f_S) = -1$:

$$a_D\,(\alpha_P x) = \frac{\pi\beta_D U_P U_S \left\{ J_{(-\delta-1)}(\xi) J_{(1+\delta)}\left[\xi \exp(-\alpha_P x)\right]\right\}}{2\alpha_P \sin(\pi\delta)\exp[\alpha_P x(1+\delta+\delta^2)]}$$

$$-\frac{\pi\beta_D U_P U_S \left\{ J_{(1+\delta)}(\xi) J_{(-\delta-1)}\left[\xi \exp(-\alpha_P x)\right]\right\}}{2\alpha_P \sin(\pi\delta)\exp[\alpha_P x(1+\delta+\delta^2)]} \qquad (4.3.19)$$

2. $f_P = f_S + f_D$, $\mathrm{sign}(f_P - f_S) = +1$:

$$a_D\,(\alpha_P x) = \frac{\pi\beta_D U_P U_S \left\{ I_{(1-\delta)}(\xi) I_{(\delta-1)}\left[\xi \exp\,(-\alpha_P x)\right]\right\}}{2\alpha_P \sin(\pi\delta)\exp[\alpha_P x(1-\delta+\delta^2)]}$$

$$-\frac{\pi\beta_D U_P U_S \left\{ I_{(\delta-1)}(\xi) I_{(1-\delta)}\left[\xi \exp\,(-\alpha_P x)\right]\right\}}{2\alpha_P \sin(\pi\delta)\exp[\alpha_P x\,(1-\delta+\delta^2)]} \qquad (4.3.20)$$

The amplitude distributions, which are inherent in the difference-frequency acoustic wave components and normalized by the factor $\pi\ \beta_D U_P U_S/(\,2\,\alpha_P\,)$, for the same pairs of the normalized acoustic wave amplitudes ξ are presented in Figs.4.4 and 4.5.

4.4 Estimating the frequency potentials peculiar to a multi-channel direct optical spectrum analysis with a novel acousto-optical cell

Potential frequency limitations can be analyzed within nonlinear acoustic mechanisms of collinear heterodyning. Without the loss of generality, it is possible

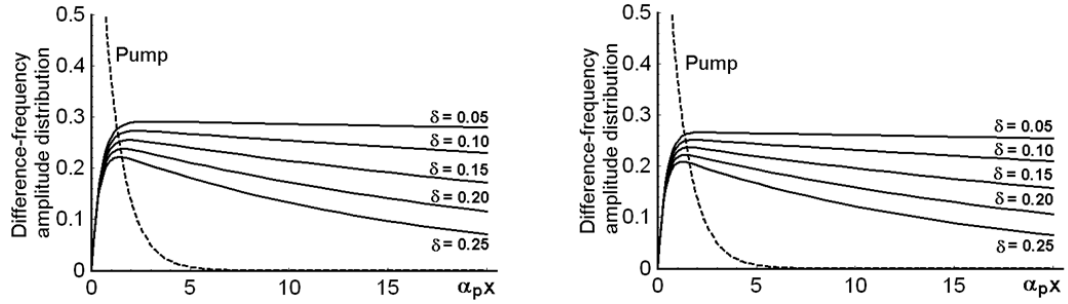

(a) $\xi = 0.5$ (b) $\xi = 1.0$

Figure 4.4: Normalized amplitudes for the difference-frequency acoustic waves versus the product $\alpha_P x$ when $f_S = f_P + f_D$

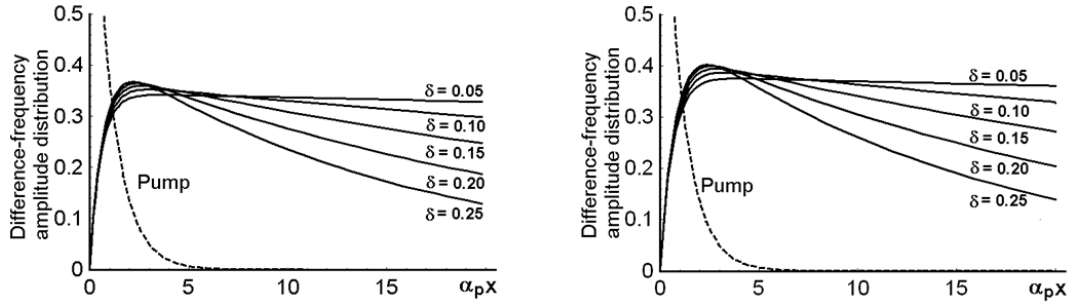

(a) $\xi = 0.5$ (b) $\xi = 1.0$

Figure 4.5: Normalized amplitudes for the difference-frequency acoustic waves versus the product $\alpha_P x$ when $f_P = f_S + f_D$

to take Eq. 4.3.19 for further analysis at length. This equation, related as before to the case of $f_S = f_P + f_D$, can be rewritten with $z = \alpha_P x$ as

$$a_D(z) = F_D \Phi(z, \delta, \xi) \tag{4.4.1a}$$

$$F_D = \frac{\pi \beta_D U_P U_S}{2\alpha_P} \tag{4.4.1b}$$

$$\Phi(z, \delta, \xi) = \frac{J_{(-\delta-1)}(\xi) J_{(1+\delta)}[\xi \exp(-z)]}{\sin(\pi\delta) \exp[z(1+\delta+\delta^2)]} - \frac{J_{(1+\delta)}(\xi) J_{(-\delta-1)}[\xi \exp(-z)]}{\sin(\pi\delta) \exp[z(1+\delta+\delta^2)]} \tag{4.4.1c}$$

At this stage, the coordinate z_m of a maximum of the amplitude function $\Phi(z, \delta, \xi)$ must be found. For this purpose, one must analyze the condition $[d\Phi(z_m, \delta, \xi)/dz] = 0$. The condition of an existing maximum for $\Phi(z, \delta, \xi)$ takes the form

$$J_{(-1-\delta)}(\xi)\left\{\delta^2 J_{(1+\delta)}[\xi\exp(z_m)] + \xi\exp(z_m)J_{(\delta)}[\xi\exp(z_m)]\right\} - J_{(1+\delta)}(\xi)$$
$$\times\left\{\delta^2 J_{(-1-\delta)}[\xi\exp(z_m)] - \xi\exp(z_m)J_{(-\delta)}[\xi\exp(z_m)]\right\} = 0 \qquad (4.4.2)$$

This condition can be easily analyzed numerically by considering δ and z_m as the independent and dependent variables, respectively, while ξ plays the role a discrete independent parameter. One can find from Eq. 4.4.2 that

$$z_m(\delta, \xi = 0.5) \approx 2.66 - 2.1\times10^{-4}\delta^{-2} + 0.0405\delta^{-1} - 8.17\delta + 10.3\delta^2 \quad (4.4.3a)$$
$$z_m(\delta, \xi = 1.0) \approx 2.587 - 6\times10^{-6}\delta^{-2} + 0.0016\delta^{-1} - 8.26\delta + 11.4\delta^2 \quad (4.4.3b)$$

see Fig. 4.6(a). These formulas are rather important because they make it possible to estimate potential frequency limitations for optical spectrum analysis.

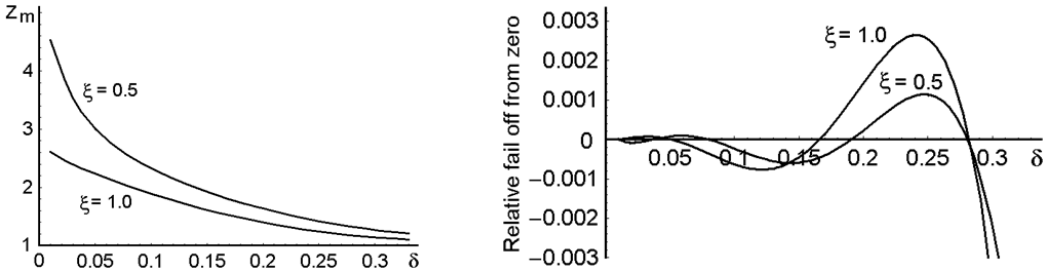

(a) (b)

Figure 4.6: In figure (a), plots determine the coordinate z_m as an approximate function of the frequency ratio δ from numerical solution to Eq. 4.4.2, whereas in (b), the curves characterize the relative accuracy of approximate plots in Fig. 4.6(a).

Substituting the obtained $z_m(\delta, \xi)$ into Eq. 4.4.2 allows, first, to estimate the accuracy of the performed approximations. Figure 4.6(b) illustrates the closeness of the derivative $d\Phi[z_m(\delta, \xi), \delta, \xi]/dz$ to zero in terms of its relative fall off from

zero for two particular cases of $\xi = 0.5$ and $\xi = 1.0$. One can see from Fig. 4.6(b) that the maximal value of an error does not exceed 0.3% within $\delta \in [0.01; 0.30]$. Then, Figs. 4.4 and 4.5 exhibit a nonuniformity of distributing signals associated with various difference-frequency acoustic components inside the cell, so that a larger non-uniformity is associated with the component of a higher value of δ. Thus, one can take the upper-difference frequency component and restrict itself by an upper value δ_u of the parameter δ. Then, substituting the obtained $z_m(\delta_U, \xi)$ into $\Phi(z, \delta, \xi)$ makes it possible to formulate the requirement to the cell's optical aperture. One can see it as follows: decreasing the normalized acoustic field distribution down to a level of -3 dB along the cell's optical aperture at a point $z_D(\delta_U, \xi)$ gives the equality

$$\Phi^2[z_D(\delta_U, \xi), \delta_U, \xi] = 0.5\Phi^2[z_m(\delta_U, \xi), \delta_U, \xi] \tag{4.4.4}$$

in terms of the intensities. In fact, the value of $z_D(\delta_U, \xi)$ determines the total geometric length $x_D(\delta_U, \xi)$ of acousto-optical cell with the collinear wave heterodyning. Then, one can explain $x_{m,D} = \alpha_P^{-1} z_{m,D}$ and obtain

$$D = x_D(\delta_U, \xi) - x_m(\delta_U, \xi) \tag{4.4.5}$$

where D is the really operating part of the cell's optical aperture available for parallel optical processing at given ξ and some range of the parameter δ. Nevertheless, it is seen from Figs. 4.4 and 4.5 that the normalized intensity distributions $\Phi^2(z, \delta, \xi)$ are the obviously decreasing functions of the parameter δ. As a result, similar dependences on δ lead to a nonuniformity of distributing signals associated with various difference-frequency components inside the cell. Moreover, this nonuniformity is as large as the corresponding parameter δ is high, so that the lowest magnitude δ_L of the parameter δ leads to almost uniform acoustic signal distribution along the cell's optical aperture. Together with this, Figs. 4.4 and 4.5 show that the parameter δ is as high, as the absolute maximum of the corresponding dependence is low, and consequently, the corresponding frequency components

have to be adequately preamplified. Under these circumstances, one can suggest the following criterion for such a pre-amplification, namely, one equalizes various frequency components in a central vicinity of the above-noted operating part D inherent in the cell's optical aperture. In so doing, one can suggest re-normalizing maximal intensity determined by the expression

$$\Phi_m^2[z_m(\delta,\xi),\delta,\xi,G] = \frac{G}{z_m(\delta,\xi)}\Phi^2[z_m(\delta,\xi),\delta,\xi] \tag{4.4.6}$$

with possible linear gain G, whose magnitude can be taken rather arbitrary. The corresponding distributions, both allowing δ_U up to 0.35 and δ_L down to 0.05, are presented in Fig 4.7 in the particular case of, for instance, $G = 4$. This diagram illustrates the simplest possibility of the above-noted equalizing the frequency components involved.

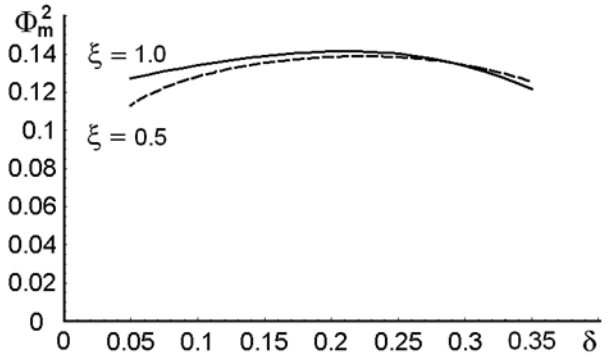

Figure 4.7: Renormalized maximal intensities $\Phi_m^2\,[Z_m(\delta),\delta,\xi]$ versus the parameter δ with $G = 4$: the dashed line is for $\xi = 0.5$, whereas the solid line is for $\xi = 1.0$.

Then, one can consider the renormalized spatial intensity distributions

$$\Phi_0^2(z,\delta,\xi) = \frac{G}{z_m(\delta)}\Phi^2(z,\delta,\xi) \tag{4.4.7}$$

along the cell's aperture. These distributions are depicted in Fig. 4.8 in the same particular case of $G = 4$ as before, together with the magnitudes $\delta_U = 0.17$ and $\delta_L = 0.034$, also taken, for example, in a view of the further consideration.

Taking into account Eq. 4.4.4, one can find from Fig. 4.8 that the really operating part D of the cell's optical aperture available for parallel optical pro-

cessing in Eq. 4.4.5 is practically independent on the magnitude of ξ. Very slight dependence on ξ manifests itself mainly in concrete localization of D within total aperture of the cell. However, this dependence is rather weak as it follows from the data in Fig. 4.8 , so that potentially it could be neglected in practice.

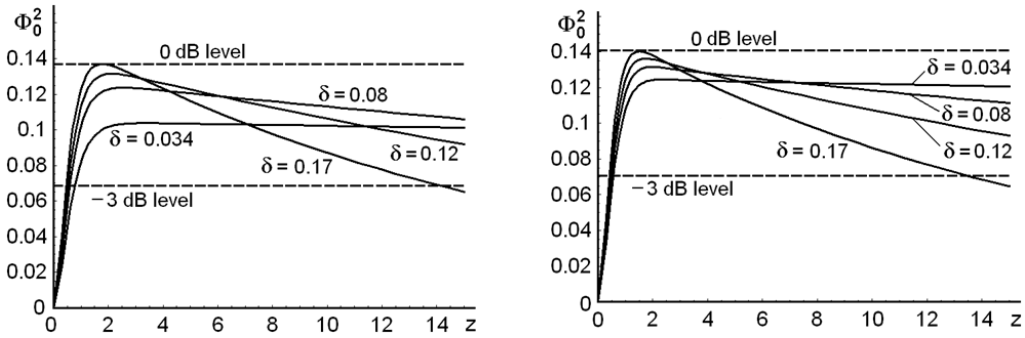

(a) $\xi = 0.5$ (b) $\xi = 1.0$

Figure 4.8: Renormalized spatial intensity distributions $\Phi_0^2(z, \delta, \xi)$ along the cell's aperture with G=4 for various δ.

At this point, an opportunity exists to simplify the process of determining the value of $x_D(\delta_U, \xi)$. In so doing, one rewrites Eq. 4.4.1c as $\Phi(z, \delta, \xi) = \Phi_1 + \Phi_2$, where

$$\Phi_1(z, \delta, \xi) = \frac{J_{(-\delta-1)}(\xi) J_{(1+\delta)}[\xi \exp(-z)]}{\sin(\pi\delta) \exp[z(1+\delta+\delta^2)]} \tag{4.4.8a}$$

$$\Phi_2(z, \delta, \xi) = \frac{-J_{(1+\delta)}(\xi) J_{(-\delta-1)}[\xi \exp(-z)]}{\sin(\pi\delta) \exp[z(1+\delta+\delta^2)]} \tag{4.4.8b}$$

Comparisons of these contributions to the right from the planes $z_m(\delta)$ in two above-chosen cases of $\xi = 0.5$ and $\xi = 1.0$ are presented in Fig. 4.9 . If $\Phi_1 \to 0$, one can put $\Phi(z, \delta, \xi) \approx \Phi_2(z, \delta, \xi)$ within at least $z \geqslant 2z_m(\delta, \xi)$ in Eq. 4.4.1b and take the reduced, but well-approximated, form of Eq. 4.4.1a

$$a_{DR}(z) = -\left(\frac{\pi\beta_D U_P U_S}{2\alpha_P}\right) \frac{J_{(1+\delta)}(\xi) J_{(-\delta-1)}[\xi \exp(-z)]}{\sin(\pi\delta) \exp[z(1+\delta+\delta^2)]} \tag{4.4.9}$$

The corresponding contributions after substituting $\Phi(z, \delta, \xi) \approx \Phi_2(z, \delta, \xi)$ into

Eq. 4.4.7 (i.e., after normalizing) are presented in Fig. 4.10 with $\delta = 0.17$ in the cases of $\xi = 0.5$ and $\xi = 1.0$ under discussion.

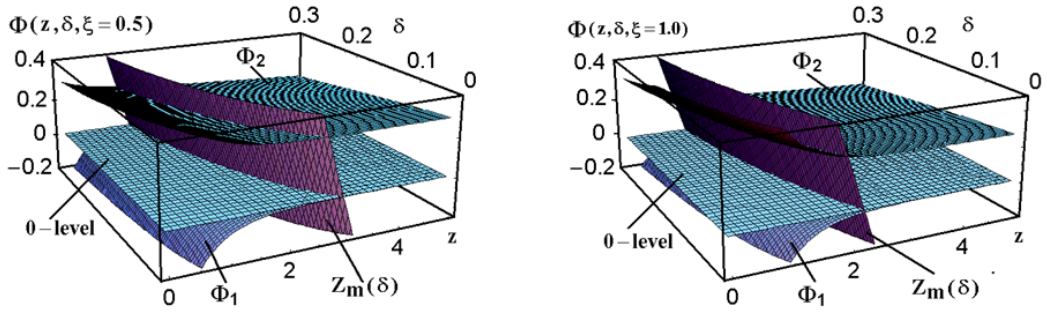

(a) (b)

Figure 4.9: Comparing the contributions of the terms Φ_1 and Φ_2 from Eq.4.4.8 to the right of the plane $z_m(\delta, \xi)$ with: (a) $\xi = 0.5$ and (b) $\xi = 1.0$. The 0 dB-levels are shown as well for a convenience.

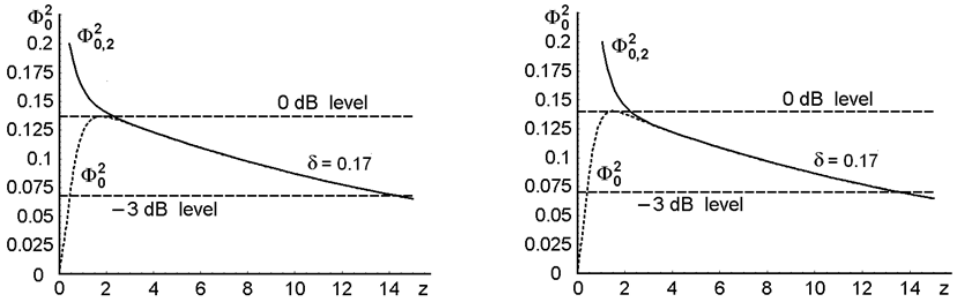

(a) $\xi = 0.5$ (b) $\xi = 1.0$

Figure 4.10: Coinciding the terms Φ_0^2 and $\Phi_{0,2}^2$ obtained from Eqs.4.4.7 and 4.4.8 to the right of the area $2z_m(\delta, \xi)$ with $G = 4$, $\delta = 0.17$ and: (a) $\xi = 0.5$ and (b) $\xi = 1.0$. The 0 dB and -3 dB levels are shown as well.

Now, directing our attention to the particular case of a KRS-5 crystalline cell with $\Gamma_0 = 10\text{dB}/(\text{cm GHz}^2)$ and practically operating optical aperture $D = 5.0$ cm and make a few practical estimations. At first, to provide higher operating frequencies inherent in the cell under consideration together with the simplicity of realizing a low-frequency pump, it looks preferable to choose an area of $f_S =$

$f_P + f_D$ and $\mathrm{sign}(f_P - f_S) = -1$ related to Eq. 4.3.19 in spite of the fact that this area is more sensitive to variations of the parameter δ (see Fig. 4.4). Applying Eq. 4.4.9 and Fig. 4.10, one can find that the upper difference-frequency about $f_{UD} \approx 250$ MHz provides approximately 3 dB level of acoustic losses along the taken optical aperture $D \approx 5.0$ cm of the cell. It should be noted at this step that the numerical estimations adduced here should be considered as rather simplified illustrations, while practically notable technical calculations must be performed much more precisely. Nevertheless, one can say that these estimations reflect the proposed principle of operation in the full measure. Because of the upper magnitude of δ in this case is $\delta_U = 0.17$, as it follows also from Fig. 4.10, and initial determination of the parameter δ gives $f_{UD}/\delta_U = f_P$, one can find that the pump frequency will be $f_P = 1470$ MHz and the upper signal frequency will be $f_{US} = 1720$ MHz. Then, one can choose the bandwidth Δf of spectrum analysis, for example, in the range of 200 MHz, which leads to the lower difference-frequency $f_{LD} = 50$ MHz restricted by the Bragg regime condition (see the corresponding estimation at the end of section 4.2). Consequently, the lower signal frequency is $f_{LS} = 1520$ MHz, and the lower magnitude of the parameter δ is $\delta_L = 0.034$. These estimations are conditioned by the relations

$$f_{UD} = f_{US} - f_P = f_P\,\delta_U \tag{4.4.10a}$$

$$f_{LD} = f_{LS} - f_P = f_P\,\delta_L \tag{4.4.10b}$$

It should be noted that direct exploitation of similar KRS-5 cell with the active optical aperture $D = 5.0$ cm at the signal frequencies of already 1000 MHz is definitely impossible because the acoustic attenuation is about 50 dB along this aperture. Nevertheless, applying the collinear acoustic wave heterodyning allows to operate on these gigahertz-range carrier frequencies. The above-mentioned non-uniformities in the distributions of signals associated with various difference-frequency components in the KRS-5 cell under consideration are illustrated in Fig. 4.8. Using Eq. 4.4.3 at the pump frequency $f_P = 1470$ MHz providing $\alpha_P = 2.485$

cm^{-}1, one can estimate with $\delta_U = 0.17$ that $z_m = 1.80$ and $x_m = 0.720$ cm for $\xi = 0.5$ as well as $z_m = 1.52$ and $x_m = 0.608$ cm for $\xi = 1.0$. Then, estimating these non-uniformities in the distributions of acoustical signals along the cell's aperture at $\delta_U = 0.17$ even graphically makes it possible to conclude from Figs. 4.8 and 4.10 that one can obtain $z_D = 14.2$ and $x_D = 5.71$ cm for $\xi = 0.5$ as well as $z_D = 13.8$ and $x_D = 5.55$ cm for $\xi = 1.0$. At this point, it is worthwhile to make two refining remarks. First, the analysis should, naturally, include considering the behavior of another frequency components inherent in the complete spectrum of the difference-frequency signal, in particular, the component with $\delta_L = 0.034$. Nevertheless, one can see from Fig. 4.8 (as well as from Figs. 4.4 and 4.5 that total irregularity inherent in this lowest-frequency component is practically insignificant even taking into account the appropriateness $z_m(\delta_L) > z_m(\delta_U)$. Second, some small part of the cell's aperture placed to the left of $z_m(\delta_U)$, which exhibit more or less "acceptable" level of signal irregularity can be also exploited practically. Thus, the really operating optical aperture D, lying between $z_m(\delta_U)$ and $z_D(\delta_U)$ for $\delta_U = 0.17$ at a level of -3 dB with the above-mentioned remarks, consists in approximately $D = 5.0$ cm [43].

4.5 Estimating the efficiency of collinear wave heterodyning

Now, the efficiency of collinear wave heterodyning in the chosen regime of a given pump intensity and coupling between signal and difference-frequency acoustic modes must be estimated. Without loss of generality, one takes Eq. 4.3.19 in the form of Eq. 4.4.1, which describes the case of $f_S = f_P + f_D$, for further analysis. At this case, the contributions involved in the term F_D from Eq. 4.4.1, which does not include any coordinate dependence contrary to the function $\Phi(z, \delta, \xi)$, are estimated. One can start from the pump losses that are described

by the factor $\alpha_P = \tilde{\Gamma}_0 f_P^2$. Usually, the acoustic attenuation factor Γ_0 is used in bibliography (see [38, 39]) measured in decibels per centimeter per gigahertz squared, but here one needs it in the form of $\tilde{\Gamma}_0$ (in seconds squared per centimeter)= $[(\ln 10)/10] \cdot 10^{-18} \cdot \Gamma_0$ [dB/(cm GHz^2)] within estimating the efficiency of collinear wave heterodyning. Then, the factor β_D, introduced in Eqs. 4.3.8 and 4.3.9, takes the form $\beta_D = 2\pi^2 V_L^{-2} \Gamma f_P f_S$. Finally, the deformation tensor $\gamma^{(L)}$, described initially by Eq. 2.2.4 in the normalized form, can be converted to the axes chosen in connection with orienting the coordinate axis x as $\vec{x} \parallel \vec{m} \parallel [1\,1\,1]$ in Eq. 4.3.4. In so doing, one can write $\gamma^{(L)} = \vec{u} \cdot \vec{q}$ for the longitudinal acoustic mode. After that, recovering the magnitudes of the vectors included into $\gamma^{(L)}$, one can explain the unique nonzero component of this tensor in dimensional form as $\gamma_j^{(11)} \equiv \gamma_j = U_j\, k_j$, where $j \in [P, S, D]$ as before, [see comments to Eq. 4.3.7]. This dimensional form represents a scalar relation as well, so that it can be inverted as $U_j = \gamma_j / k_j$,where$k_j = 2\pi f_j / V_L$. In its turn, the chosen component of deformations can be explained in terms of the corresponding acoustic power density P_j as $\gamma_j^2 = 2P_j/(\rho V_L^3)$ [33]. Exploiting these relations, one can obtain from Eq. 4.4.1 that

$$F_D^2 = \frac{\pi^2 \Gamma^2 P_P P_S}{4\tilde{\Gamma}_0^2 \rho^2 V_L^6 f_P^4} \tag{4.5.1}$$

Together with this, the left-hand side of Eq. 4.4.1a gives

$$a_D^2\,(z)\,\Phi^{-2}\,(z, \delta, \xi) = \frac{P_D}{2\pi^2 \rho V_L f_D^2} \tag{4.5.2}$$

Combining Eq. 4.5.1 and 4.5.2, one can find the power density of the difference-frequency acoustic wave

$$P_D = 4\pi^2 P_P P_S m \left(\frac{f_D^2}{f_P^4}\right) \Phi^2\,(z, \delta, \xi) \tag{4.5.3a}$$

$$m = \frac{\pi^2 \Gamma^2}{8\rho \tilde{\Gamma}_0^2 V_L^5} \tag{4.5.3b}$$

Now, one can estimate the total efficiency I of Bragg light scattering by the difference-frequency acoustic wave. In the particular case of rather weak acoustic

signals, when nonlinearity inherent in acousto-optical interaction can be omitted [33], one can use only a few terms from the corresponding expansion and write

$$I = \sin^2(qL) \approx q^2L^2 - \frac{1}{3}q^4L^4 + \cdots \tag{4.5.4a}$$

$$q \approx \pi\lambda^{-1}\sqrt{M_2\,P_D/2} \tag{4.5.4b}$$

Under natural condition $q^2L^2 << 3$, i.e. under inequality

$$P_D << 6\lambda^2/\left(\pi^2 M_2 L^2\right) \tag{4.5.5}$$

one may restrict himself by the first term on the right- hand side of Eq. 4.5.4a and rewrite Eq. 4.5.4a as $I = \pi^2 M_2 L^2 P_D/(2\lambda^2)$. Sometimes, [see for instance, Eq. **??**], it is worthwhile to exploit the parameter $\mu = (\pi^2/2)\,M_2 m$, which combines characterization of both nonlinear acoustic and linear acousto-optic properties of material under consideration. The magnitude of I determines the combined efficiency of the acousto-optical cell under consideration in terms of light scattering. This result makes it possible to characterize the contribution of acousto-optical interaction exploiting Eq. 4.5.4a in the form of

$$I_{\max} = \frac{1}{(2\lambda^2)}\pi^2 M_2 L^2 P_{D\,\max} \tag{4.5.6}$$

With a maximally allowed level $P_{D\,\max} \approx 5\cdot 10^5$ g/s^3 = 0.05 W/cm^2, obtained from Eq. 4.5.5, one can find $I_{\max} \approx 0.3$. This estimation makes it possible to consider the above-chosen level of P_D as more or less tolerable for an upper limit in a KRS-5 single crystal under the aforementioned condition given by Eq. 4.5.5. An undoubted merit of this characterization consists of practically convenient direct proportionality between the efficiency I and the power density P_D.

After that the contribution of acoustic wave mixing should be briefly analyzed. With this object in view, one can use Eqs. 4.3.19 and 4.3.20 for estimating the acoustic pump power density $P_{P\,0}$ needed to reaching a preassigned peak level of the difference-frequency power density $P_{D\,\max}$ at a given ratio $\alpha = P_S/P_{P0}$. From the start, it should be noted that a peak magnitude peculiar to the squared

coordinate dependence $\Phi_m^2\left[z_m(\delta,\xi),\delta,\xi,G\right] = \left(G\,\Phi^2\left[z_m(\delta,\xi),\delta,\xi\right]\right)/z_m(\delta,\xi)$ in, for example, Eq. 4.4.6 can be estimated as $\Phi_m^2[z_m(\delta,\xi),\delta,\xi,G] \approx 0.1$ with $G = 4$ (see Fig. 4.7). Consequently, one can find

$$P_{P0} = \frac{f_P}{2\pi\delta\Phi_m[z_m(\delta,\xi),\delta,\xi,G]}\sqrt{\frac{P_{D\,\max}}{\alpha\, m}} \tag{4.5.7}$$

In the particular case of KRS-5 single crystal, when the required magnitude of $I_{\max}$ is for instance equal to 3% (which is quite reasonable for the spectrum analysis in a small-signal linear regime), Eq. 4.5.6 gives $P_{D\,\max} \approx 3.0 \cdot 10^4$ g/s^3 $= 0.003$ W/cm^2. Then, taking $m \approx 1.1 \cdot 10^{11}$ s/g, $\alpha = 0.1$, $G = 4$, $\delta = 0.15$, $\xi = 1.0$, and $f_P = 1.5$ GHz, one can estimate from Eq. 4.5.7 the needed value of the acoustic pump power density by $P_{P0} \leqslant 0.83 \cdot 10^7$ g/s^3 $= 0.83$ W/cm^2, which is acceptable.

4.6 Conclusion

The presented data demonstrate both the possibility and the potential advantages of applying a codirectional collinear wave heterodyning to essential, about an order of magnitude or more, improvement of the frequency resolution within a multichannel parallel acousto-optical spectrum analysis of gigahertz-frequency range analog radio-wave signals. In so doing, the phenomenon of a codirectional collinear wave heterodyning has been theoretically investigated, it is taken in the particular case of mixing the longitudinal acoustic waves of finite amplitudes. The methods for estimating the total efficiency of operation and optimizing aperture parameters for the cell of a new type have been developed.

Chapter 5

General conclusions

1. The obtained experimental data make possible considering a few estimations of an advanced collinear acousto-optical filter (AOF) based on calcium molybdate ($CaMoO_4$) single-crystal. This new AOF with a 15-microsecond time-aperture operates over all the visible range exhibiting 60%-efficiency at the electric power 1.0 W. Its bandwidth, which in fact characterizes the resolution due to the well-known relation $\Delta f \equiv \delta f$ between the frequency bandwidth and the frequency resolution in the case of collinear scheme, includes two contributions. The first one does not depend on the divergence angles of optical and acoustic beams, and it prevails when these angles are under a critical angle. The second contribution dominates with really wide-angle divergence of these beams or when AOF crystal is sufficiently long; so that the bandwidth shows a quadratic growth as the divergence angles increase. Estimating that critical angle shows that it does not exceed 10 degrees when the crystal is shorter than 6 cm in length and the acoustic frequency is lower than 100 MHz.

2. The proposed technique exploiting a two-cascade algorithm of processing provides more than 5000-frequency-channels for processing analog radio-wave signals in a gigahertz-frequency range with the relative frequency resolution about 10^{-5}, which is usually unattainable for conventional direct acousto-optical methods. The obtained results reflect the fruitful character of modern approaches based on applying various non-linear phenomena to improving the performance data of

optical processing and give an appropriate example of this kind. At the moment, a few practical advantages of the presented approach can be noted. First, the proposed device does not need not additional electronic equipment for mixing the signals and selecting the resulting carrier frequency, because heterodyning can be performed directly in a cell and provides potentially the dynamic range of about 90 dB peculiar to wave processes in solids. Then, the approach under consideration decreases the required relative bandwidth of piezoelectric transducer from 50-100% at the resulting frequency within a conventional cell to 15% at the initial carrier frequency. Third, in the case of a spatially multichannel arrangement of the acousto-optical cell, the identity of neighboring spatial channels to each other can be provided by adjusting the corresponding heterodynes. Finally, one should note that the number of isotropic or crystalline materials, which are appropriate for acousto-optical cells processing signals in a gigahertz-frequency range, is definitely restricted due to fast-growing influence of square-law frequency dependence for the acoustic attenuation in solids. One can easily show that the above-discussed KRS-5 cubic crystal cannot be used for creating a conventional acousto-optical cell operating with signals whose carrier frequency exceeds about 400-500 MHz. Nevertheless, just this crystalline material, alone, can be, in principle, exploited for the control over $f_0 = 1.6$ GHz signals. Consequently, one can conclude that a two-cascade arrangement of a cell presented here allows extending the spectrum of acousto-optical materials being appropriate for direct processing of ultra-high-frequency analog radio wave signals.

List of Figures

List of Tables

References

[1] L. Brillouin, "Diffusion of light and x-rays by a transparent homogeneous body," *Ann. Phys* **17**, pp. 88–122, 1922.

[2] F. Yu, S. Jutamulia, and S. Yin, *Introduction to information optics*, Academic, 2001.

[3] N. Berg and J. Lee, *Acousto-optic signal processing: theory and implementation*, Marcel-Dekker, 1983.

[4] R. G. Gould, "The LASER, light amplification by stimulated emission of radiation," in *The Ann Arbor Conference on Optical Pumping, the University of Michigan, 15 June through 18 June 1959*, F. P.A. and R. Sands, eds., p. 128, 1959.

[5] Y. Kivshar and G. Agrawal, *Optical solitons: from fibers to photonic crystals*, Academic Press, 2003.

[6] N. Akhmediev and A. Ankiewicz, *Solitons: nonlinear pulses and beams*, Chapman & Hall, 1997.

[7] A. Shcherbakov and A. Aguirre Lopez, "Wave multiplication of binary encoded data exploiting solitary multi-pulse non-collinear three-wave coupled states," *J. Opt. A: Pure Appl. Opt.* **8**, pp. 464–472, 2006.

[8] A. Shcherbakov, A. Bliznetsov, A. Luna Castellanos, and D. Sanchez Lucero, "Acousto-optical spectrum analysis of ultra-high-frequency radio-wave analogue signals with an improved resolution exploiting the collinear

acoustic wave heterodyning," *Optik - International Journal for Light and Electron Optics* **121**(16), pp. 1497–1506, 2010.

[9] A. Shcherbakov, D. Sanchez Lucero, A. Luna Castellanos, and O. Belokurova, "Direct multi-channel optical spectrum analysis of radio-wave signals using collinear wave heterodyning in the single acousto-optical cell," *Journal of Optics* **12**, pp. 045203–+, apr 2010.

[10] R. Dixon, "Acoustic diffraction of light in anisotropic media," *IEEE Journal of Quantum Electronics* **3**, pp. 85–93, feb 1967.

[11] C. Cooper, *Physics*, Fitzroy Dearborn, 2001.

[12] N. Uchida and N. Niizeki, "Acousto-optic deflection materials and techniques," *Proc. IEEE* **61**, pp. 1073–1092, Aug 1973.

[13] J. Nye, *Physical properties of crystals: their representation by tensors and matrices*, Clarendon Press, 1985.

[14] Y. Sirotin and M. Shaskol'skaya, *Fundamentals of crystal physics*, Mir Publishers, 1982.

[15] T. Narasimhamurty, *Photoelastic and electro-optic properties of crystals*, Plenum Press, 1981.

[16] C. Kittel, *Introduction to solid state physics*, Wiley, 2005.

[17] "Magnetostrictive versus piezoelectric transducers for power ultrasonic applications," tech. rep., Blackstone NEY Ultrasonics, Inc., 9 North Main Street.

[18] S. O. R. Moheimani and A. J. Fleming, "Fundamentals of piezoelectricity," in *Piezoelectric Transducers for Vibration Control and Damping*, M. J. Grimble and M. A. Johnson, eds., pp. 9–35, Springer London, 2006.

[19] A. L. Kholkin, N. A. Pertsev, and A. V. Goltsev, "Piezoelectricity and crystal symmetry," in *Piezoelectric and Acoustic Materials for Transducer*

Applications, A. Safari and E. K. Akdoğan, eds., pp. 17–38, Springer US, 2008.

[20] J. N. Lee, "Optical modulators," in *The Handbook of photonics*, M. C. Gupta, ed., ch. 9, pp. 393–434, CRC Press, 1997.

[21] S. Bhagavantam, "Photo-elastic effect in crystals," *Proc. Mathematical Sciences* **16**(6), pp. 359–365, 1942.

[22] T. M. Smith and A. Korpel, "Measurement of light-sound interaction efficiency in solids," *IEEE J. Quantum Electron.* **QE-1**, pp. 283–284, 1965.

[23] E. I. Gordon, "A review of acoustooptical deflection and modulation devices," *Appl. Opt.* **5**, pp. 1629–1639, Oct 1966.

[24] R. W. Dixon, "Photoelastic Properties of Selected Materials and Their Relevance for Applications to Acoustic Light Modulators and Scanners," *Journal of Applied Physics* **38**, pp. 5149–5153, Dec. 1967.

[25] M. Bass, C. Decusatis, V. Mahajan, C. MacDonald, G. Li, and E. Stryland, *Handbook of Optics, Third Edition Volume V: Atmospheric Optics, Modulators, Fiber Optics, X-Ray and Neutron Optics*, McGraw-Hill, 2009.

[26] M. Gottlieb, C. Ireland, and J. Ley, *Electro-optic and acousto-optic scanning and deflection*, Optical engineering, M. Dekker, 1983.

[27] A. Yariv and P. Yeh, *Optical waves in crystals: propagation and control of laser radiation*, John Wiley and Sons, 2002.

[28] I. Egorov, K. Naumov, and V. Ushakov, *Acousto-optic correlators and spectrum analyzers: new techniques for signal processing*, SPIE Optical Engineering Press, 1997.

[29] J. N. Lee and A. Vanderlugt, "Acoustooptic signal processing and computing," *Proc. IEEE* **77**, pp. 1528–1557, Oct. 1989.

[30] R. Klein and B. Cook, "A unified approach to ultrasonic light diffaction," *IEEE Trans, on sonics and ultrasonics* **SU-14**(3), pp. 123–134, 1967.

[31] G. Agrawal, *Nonlinear fiber optics*, Academic Press, 2007.

[32] V. Balakshy, V. Parygin, and L. Chrkov, *Physical principles of acousto-optics*, Radio I Svyaz, 1985.

[33] A. Korpel, *Acousto-optics*, Marcel-Dekker, 1997.

[34] M. Abramowitz and I. Stegun, *Handbook of Mathematical Functions with Formulas, Graphs, and Mathematical Tables*, vol. 55.

[35] J. Tucker and V. Rampton, *Microwave ultrasonics in solid state physics*, North-Holland, 1972.

[36] D. Pinnow, "Guide lines for the selection of acoustooptic materials," *IEEE Journal of Quantum Electronics* **6**, pp. 223–238, Apr 1970.

[37] A. S. Shcherbakov, J. Maximov, D. S. Lucero, and K. J. Sanchez Perez, "Characterizing the performances of an advanced acousto-optical filter exploiting the collinear calcium molybdate crystalline cell," **7917**(1), p. 791715, 2011.

[38] G. Gurzadyan, V. Dmitriev, and D. Nikogosyan, *Handbook of nonlinear optical crystals*, Springer, 1999.

[39] A. Blistanov, *Crystals for quantum and nonlinear optics*, MISIS, 2007.

[40] A. Norris, "Finite amplitude waves in solids," in *Nonlinear acoustics*, M. Hamilton and D. Blackstock, eds., ch. 9, pp. 263–277, Academic Press, 1998.

[41] V. Kludzin and V. Molotok, "Experimental characteristics of the elastic nonlinearity in KRS-5 and $NaBi(MoO_4)O_2$ crystals," *in 1994 IEEE Ultrasonic Symposium Proceedings, (Cannes, France)* **2**, pp. 851–854, 1994.

[42] M. Abramowitz and I. Stegun, *Handbook of Mathematical Functions with Formulas, Graphs, and Mathematical Tables*, vol. 55.

[43] A. S. Shcherbakov, J. Maximov, A. M. Bliznetsov, and K. J. Sanchez Perez, "Potentials of acousto-optical spectrum analysis on a basis of a novel algorithm of the collinear wave heterodyning in a large-aperture KRS-5 crystalline cell," *Optical Engineering* **50**, pp. 034002–+, Mar. 2011.